Journal of Medicinal Chemistry Article

J. Med. Chem. **2010,** *53,* 6851–6866 **6851**
DOI: 10.1021/jm901894c

New Anthracenedione Derivatives with Improved Biological Activity by Virtue of Stable Drug−DNA Adduct Formation

Oula C. Mansour,[†] Benny J. Evison,[†] Brad E. Sleebs,[‡] Keith G. Watson,[‡] Abraham Nudelman,[§] Ada Rephaeli,[∥] Damian P. Buck,[⊥] J. Grant Collins,[⊥] Rebecca A. Bilardi,[†] Don R. Phillips,[†] and Suzanne M. Cutts*[,†]

[†]*Department of Biochemistry, La Trobe University, Victoria 3086, Australia,* [‡]*The Walter and Eliza Hall Institute of Medical Research, Parkville, Victoria, 3052, Australia,* [§]*Chemistry Department, Bar-Ilan University, Ramat-Gan, 52900, Israel,* [∥]*Sackler Faculty of Medicine, Felsenstein Medical Research Center, Tel-Aviv University, Petach-Tikva 49100, Israel, and* [⊥]*School of Physical, Environmental and Mathematical Sciences, University of New South Wales, Australian Defence Force Academy, ACT 2600, Australia*

Received December 22, 2009

Mitoxantrone is an anticancer agent that acts as a topoisomerase II poison, however, it can also be activated by formaldehyde to form DNA adducts. Pixantrone, a 2-aza-anthracenedione with terminal primary amino groups in its side chains, forms formaldehyde-mediated adducts with DNA more efficiently than mitoxantrone. Molecular modeling studies indicated that extension of the "linker" region of anthracenedione side arms would allow the terminal primary amino greater flexibility and thus access to the guanine residues on the opposite DNA strand. New derivatives based on the pixantrone and mitoxantrone backbones were synthesized, and these incorporated primary amino groups as well as extended side chains. The stability of DNA adducts increased with increasing side chain length of the derivatives. A mitoxantrone derivative bearing extended side chains (**7**) formed the most stable adducts with ∼100-fold enhanced stability compared to mitoxantrone. This finding is of great interest because long-lived drug−DNA adducts are expected to perturb DNA-dependent functions at all stages of the cell cycle.

Introduction

Numerous classes of anticancer drugs are represented by compounds that form stable chemical bonds with DNA. A large number of such compounds have been synthesized and tested for anticancer activity, and many of them are in clinical use.[1] The cytotoxicity of these drugs is mainly caused by an apoptotic response, which is triggered by the formation of DNA adducts.[2]

Mitoxantrone (**1**, Figure 1) is a synthetic anticancer agent that belongs to the anthracenedione class of compounds.[3,4] The initial motive behind its synthesis was to find an anthracycline analogue with the same potent cytotoxicity but with less cardiotoxicity.[3,5] **1** lacked the severe cardiotoxic side effects of the anthracyclines and has subsequently been used against a wide range of solid tumors and myeloid cancers.[6] As an anthracycline analogue, **1** maintains the planar ring structure that allows intercalation between base pairs of DNA.[7,8] **1** is classified as a typical intercalating agent that accumulates in the nucleus where it acts as a topoisomerase II poison,[6] thereby inhibiting the topological modification of DNA. The drug blocks the strand scission step of the topoisomerase II catalytic cycle, stabilizes the "cleavable complex", and leads to the generation of DNA double-strand breaks (DSB[a]).[9] Although **1** exhibits lower toxicity compared to doxorubicin, it still causes a range of side effects, including myelosuppression and mild cardiotoxicity.[6,10]

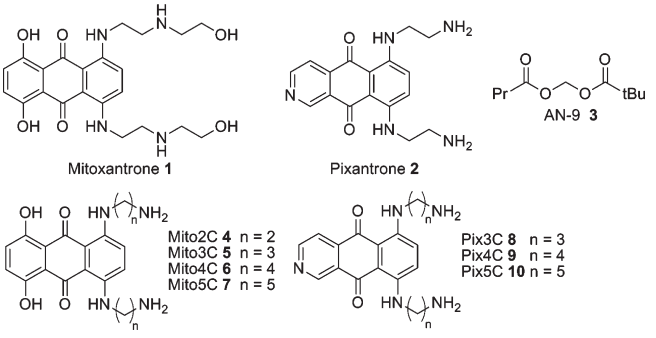

Figure 1. Chemical structures of AN-9 **3** and the anthracenediones studied. Mitoxantrone **1**; Pixantrone **2**; **1**-derived analogues **4**−**7**; **2**-derived analogues **8**−**10**.

1, like doxorubicin, can be activated by formaldehyde to generate covalent **1**−DNA adducts.[11−13] These adducts were originally detected by interstrand cross-linking assays as they stabilize duplex DNA.[12] Both formaldehyde and **1** were required to form the adducts, confirming a key role for formaldehyde in activating **1**.[12] Production of formaldehyde is relatively more active in cells of myeloid origin[14] as well as in solid tumors where it is generated from biologically available polyamines.[15,16] These findings may explain why **1** is more effective against myeloid and solid tumors.

1−DNA adducts have a half-life of approximately 50 min, indicating that the adducts are intrinsically unstable. An energy-minimized model of **1**−DNA adducts demonstrated that these adducts were likely to be mediated by a linkage between the secondary amino portion of one side arm of **1** and the exocyclic N-2 of guanine,[17] with the drug chromophore

*To whom correspondence should be addressed. Phone: +61-03-9479-1517. Fax: +61-03-9479-2467. E-mail: s.cutts@latrobe.edu.au.

[a] Abbreviations: DSB, double-strand breaks; MTT, 3-(4,5-dimethylthiazol-2-yl)-2,5-diphenyltetrazolium bromide; TE, Tris-EDTA buffer; TC, transcription buffer; CI, combination index.

Published on Web 09/22/2010

intercalated between C and G residues of a CpG dinucleotide. The substitution of the secondary amino by a primary amino function has been suggested[18,19] based on studies of the DNA binding mode of other formaldehyde activated compounds.[13,20,21]

Pixantrone **2** (Figure 1), a novel 2-aza-anthracenedione with primary amino groups in its side chains, has recently demonstrated significant anticancer efficacy. The drug fails to induce any detectable cardiotoxicity and is now in phase III clinical trials for the treatment of aggressive non-Hodgkin's lymphoma.[22,23] It was recently demonstrated that formaldehyde-activated **2**, due to the primary amino groups incorporated into its side arms, formed stable DNA adducts much more effectively than **1**, forming a covalent linkage at CpG sequences in DNA with at least one accessible guanine at the N-2 position.[24,25] On the basis of this finding and on the energy-minimized model described above, anthracenedione derivatives were designed in an attempt to develop compounds with better DNA reactivity, cross-linking potential, and stability. The side arm moieties of **1** were replaced by methylene tethers, of varying lengths, with terminal primary amine functionalities to yield compounds **4**−**7** (Figure 1). Similarly, the side chains of **2** were extended to yield the three derivatives **8**−**10** (Figure 1).

Each derivative was initially tested for its capacity to bind covalently with DNA in the presence of formaldehyde. The stability of each drug−DNA lesion was subsequently explored and their DNA sequence specificity determined. The cell growth inhibition effects of **1** derivatives in combination with the formaldehyde-releasing prodrug AN-9 **3**[26] (Figure 1) were also evaluated as a preliminary study.

Results

Drug Concentration Dependence of Adduct Formation Displayed by Formaldehyde-Activated Anthracenediones. Each anthracenedione was initially tested in a cross-linking assay for the capacity to form DNA adducts in the presence of formaldehyde. When anthracyclines and anthracenediones are covalently bound to DNA, duplex DNA is stabilized and exhibits an altered thermal melting profile where the midpoint melting temperature is increased.[27] The optimal denaturation temperature for the detection of anthracenedione derivative−DNA adducts was determined as 52 °C (data not shown). DNA was initially reacted with a range of increasing concentrations of each drug in the presence of formaldehyde. Samples were subjected to a phenol/chloroform cleanup procedure to remove unbound and intercalated drug and denatured in formamide before separation by electrophoresis. The phosphorimage in Figure 2A shows that all **1**-based compounds formed high levels of stabilized double-stranded DNA (dsDNA) at low concentrations with the exception of **1** itself, which required around 50 μM to achieve the same level of stabilization (Figure 2C) as previously documented.[24] **7** was slightly more potent than the other derivatives, with 90% dsDNA stabilization achieved at 7.5 μM, while at the same concentration, **6** and **5** formed 70% and 45% dsDNA stabilization, respectively. In contrast, **2**-based derivatives were all less effective than **2** and did not form high levels of DNA adducts (Figure 2B). At 7.5 μM, **2** yielded 100% dsDNA stabilization, while at the same concentration, **8**−**10** caused less than 20% dsDNA stabilization. **10** was slightly more effective in stabilizing dsDNA than the other derivatives (Figure 2D).

Time Dependence of Adduct Formation Displayed by Formaldehyde-Activated Anthracenediones. The time dependence of adduct formation by the derivatives was subsequently investigated. Anthracenediones (7.5 μM and 25 μM for all **1** and **2** derivatives, respectively) were reacted with end-labeled pCC1 DNA and 2 mM formaldehyde. All derivatives formed DNA adducts in a time-dependent manner (Figure 3A,B). **7** achieved a maximal level of dsDNA stabilization, reaching 100% within 10 h while **1** exhibited significantly lower reactivity, failing to stabilize any detectable dsDNA even at 24 h. Formaldehyde-activated **5** and **6** stabilized an intermediate level of dsDNA at 20 and 40% dsDNA, respectively (Figure 3C). In contrast to the **1** group of derivatives where **7** was the more reactive derivative, **2** was the most active of its group, with 100% dsDNA stabilization formed in the first 6−7 h (Figure 3D). All **2** derivatives did not reach more than 50% dsDNA stabilization in the 24 h period of incubation (Figure 3D).

Formaldehyde Concentration-Dependence of Adduct Formation Displayed by Formaldehyde-Activated Anthracenediones. To confirm that DNA adducts formed by **1**, **2**, and their derivatives were dependent on formaldehyde, a formaldehyde concentration-dependence study was performed. All derivatives (15 μM) were reacted overnight with DNA and a range of increasing concentrations of formaldehyde (0−3 mM). **1**, **2**, and their derivatives did not form adducts in the absence of formaldehyde, confirming the absolute requirement for formaldehyde in mediating a covalent aminal linkage to DNA. The formation of DNA adducts induced by **1**, **2**, and the derivatives were clearly dependent on formaldehyde concentration with increasing levels of adducts in the presence of increasing levels of formaldehyde (Figure 4A,B). **7** was again the most effective derivative in forming stable DNA adducts, followed by **6** and then **5** (Figure 4C). In contrast, **2** derivatives were all less effective than **2**, with **10** being more reactive than the other derivatives (Figure 4D).

Stability of Adducts Induced by Formaldehyde-Activated Anthracenediones. One of the most desirable attributes of the new derivatives was the ability to form stable drug−DNA adducts at a physiologically relevant temperature. To ascertain the stability of the derivatives, drug−DNA adducts were generated by reacting those derivatives at a concentration that would initially yield 60−90% dsDNA stabilization. Interestingly, the stability of adducts increased dramatically with increasing side arm length, with **1** derivatives displaying slightly better stability than **2** derivatives (Figure 5A,B). The half-life of **7** was more than 2.5 days, while that of **1** was less than 60 min (Figure 5C and summarized in Table 1). **6** and **5** exhibited half-lives of 30 and 14 h, respectively (Figure 5C; Table 1). The same trend was seen with **2** derivatives, which exhibited the following half-lives: approximately 35 h for **10**, 16 h for **9**, 13 h for **8**, and 2 h for **2** (Figure 5D; Table 1). As **7** displayed exceptionally high DNA adduct stability, an extended stability study was performed over a period of 12 days. Samples were incubated for defined time periods up to 12 days at 37 °C. There was a slow loss of adducts with an extended half-life (Figure 5E).

pH Dependence of Adduct Formation by Formaldehyde-Activated Anthracenediones. The pH dependence of formation of adducts by **1** and **2** derivatives was also established. Different concentrations of derivatives that were expected to yield between 40 and 60% dsDNA stabilization at neutral pH were used (Figure 6A,B). **1**−DNA adduct formation was pH dependent, with neutral pH required for optimal formation as previously demonstrated.[24] In contrast, **1** derivatives

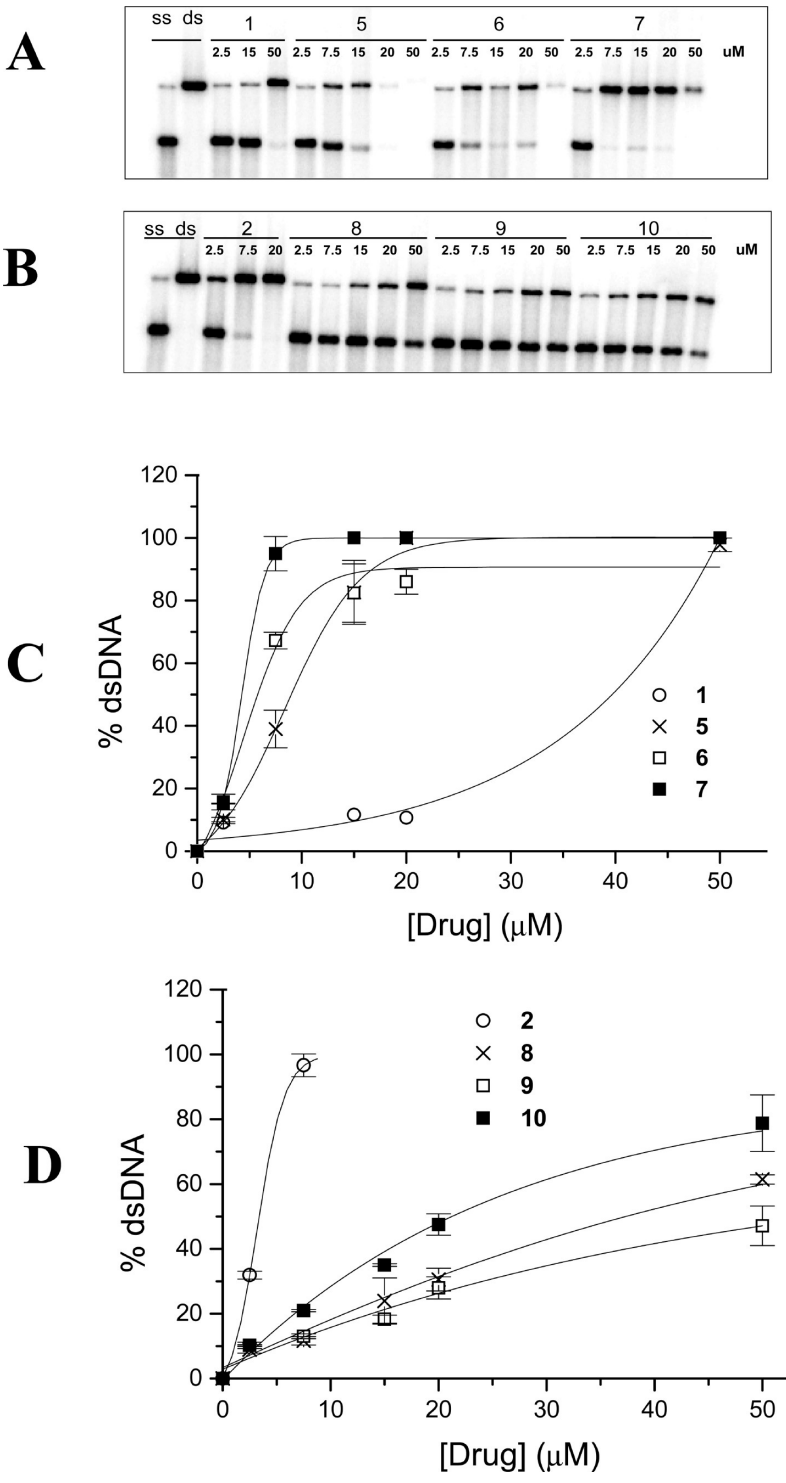

Figure 2. Drug concentration dependence of adduct formation displayed by **1** and **2** derivatives. (A,B) Anthracenediones (0−50 μM) were reacted with pCC1 DNA (25 μM_{bp}) in the presence of 2 mM formaldehyde in 1× PBS for 12 h at 37 °C. Control ssDNA represents unreacted DNA that was thermally denatured while the dsDNA control was not subjected to thermal denaturation. Images shown are representative of those obtained from each of two independent experiments. (C) Quantitation of gel (A). The percentage of dsDNA stabilized by formaldehyde-activated **1** (○), **5** (×), **6** (□), and **7** (■) was quantitated and is expressed as a function of drug concentration. (D) Quantitation of gel (B). The percentage of dsDNA stabilized by formaldehyde-activated **2** (○), **8** (×), **9** (□), and **10** (■) was quantitated and is expressed as a function of drug concentration. Results shown are the average of two independent experiments, with error bars representing the range.

were not pH dependent, although slightly lower levels of adducts typically formed under alkaline conditions and there appeared to be a slight increase of the optimal pH with decreasing side chain length (Figure 6C). Adduct formation with **2** and related derivatives were also essentially independent of pH (Figure 6D).

DNA Adduct Formation Studies with Derivative 4. **7** was clearly more effective than **1** in rapidly forming stable, non-pH dependent DNA adducts at low concentrations. In contrast, **2**, with a shorter side chain length, proved to be more effective than **2** derivatives in forming DNA adducts. **4**, a new derivative based on the **1** backbone but with two

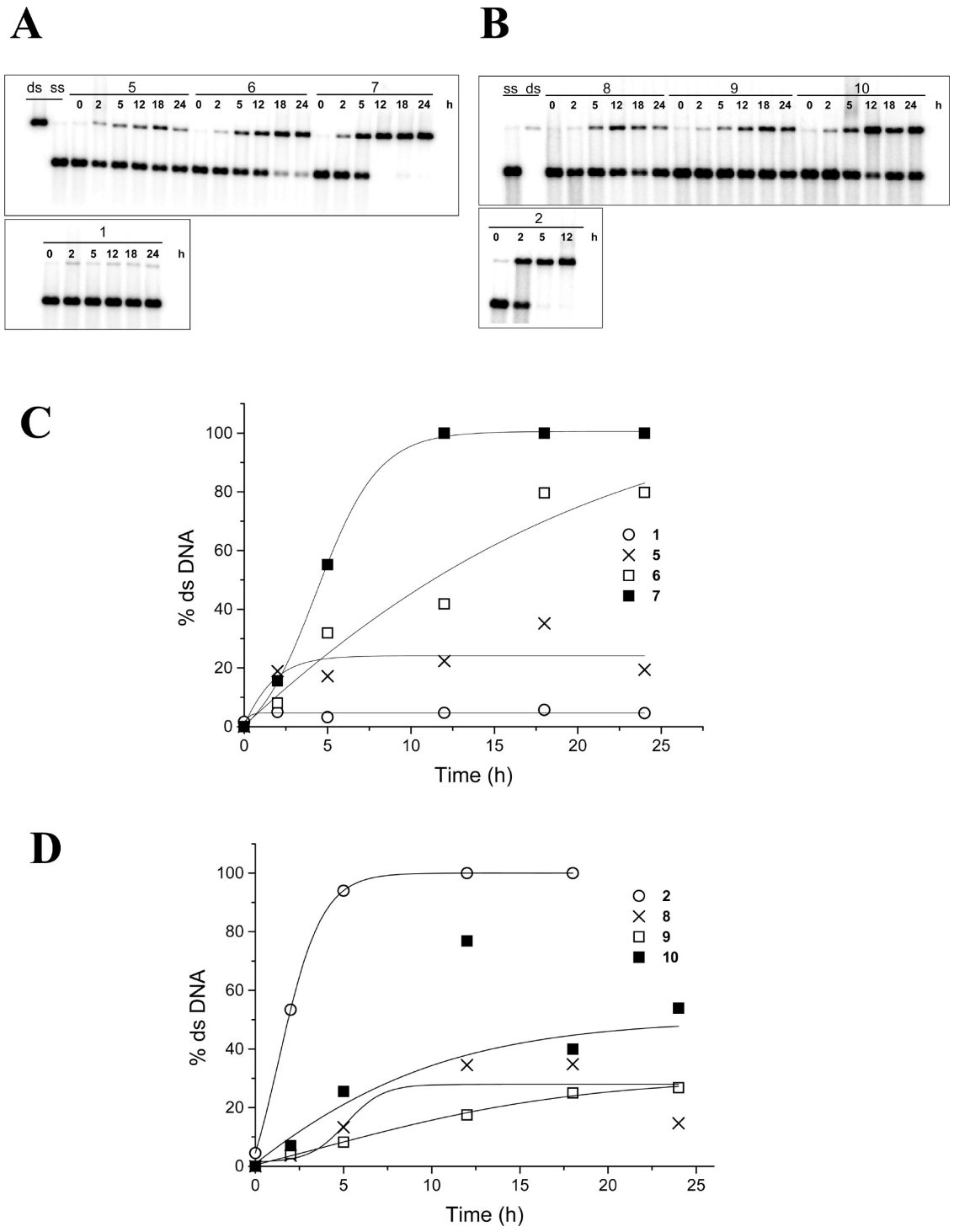

Figure 3. Time dependence of adduct formation displayed by **1** and **2** derivatives. A 7.5 μM concentration (A) and 25 μM concentration (B) were used with all compounds which were reacted with pCC1 DNA (25 μM_{bp}) and 2 mM formaldehyde in PBS at 37 °C for increasing time periods up to 24 h as indicated. (C) Quantitation of gel (A). The percentage of dsDNA stabilized for **1** (○), **5** (×), **6** (□), and **7** (■) reacted DNA samples was quantitated and expressed as a function of time. (D) Quantitation of gel (B). The percentage of dsDNA stabilized for **2** (○), **8** (×), **9** (□), and **10** (■) reacted DNA samples was quantitated and expressed as a function of time.

methylene groups in each side chain, was therefore synthesized to enable direct comparison to **2** and determine if shorter chain length corresponds to a greater efficiency of adduct formation for each backbone studied.

4 was compared to **7** and **2** in drug concentration dependence experiments. All compounds behaved similarly, forming DNA adducts at relatively low concentrations (Figure 7A). At a concentration of 2.5 μM, the three compounds attained approximately 40% dsDNA stabilization. The formaldehyde concentration dependence was then examined for **4**, and **7** was used for comparison (both compounds at 15 μM). Both compounds showed a similar dependence on formaldehyde concentration, with no adducts formed in its absence. Less than 1 mM formaldehyde was needed for both drugs to achieve 50% dsDNA stabilization, and 100% was achieved with 2 mM formaldehyde (Figure 7B). Stability studies indicated that **4**

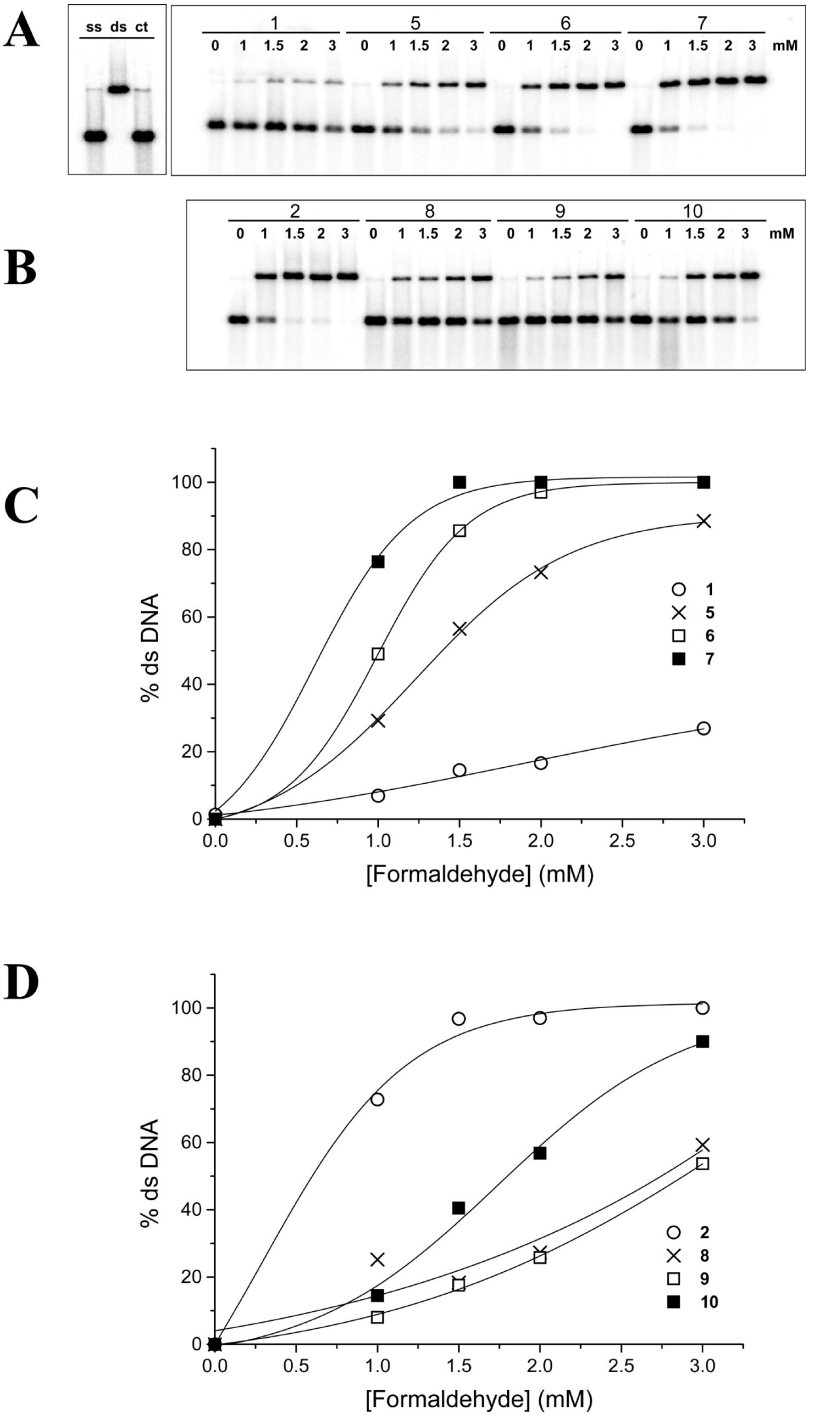

Figure 4. Formaldehyde concentration dependence of adduct formation displayed by **1** and **2** derivatives. (A,B) Drugs (at 15 μM concentration) were reacted with pCC1 DNA (25 μM_{bp}) and increasing concentrations of formaldehyde ranging from 0 to 3 mM in PBS for 16 h at 37 °C. Control ssDNA is the unreacted DNA thermally denatured, while the dsDNA control is the unreacted native dsDNA. A third control (ct) is the no-drug reacted DNA incubated with 2 mM formaldehyde. (C) Quantitation of gel (A). The percentage of dsDNA stabilized for **1** (○), **5** (×), **6** (□), and **7** (■) reacted DNA samples was quantitated and expressed as a function of formaldehyde concentration. (D) The percentage of dsDNA stabilized for **2** (○), **8** (×), **9** (□), and **10** (■) reacted DNA samples was quantitated and expressed as a function of formaldehyde concentration.

adducts were rapidly lost (half-life approximately 2.3 h) relative to **7** adducts (half-life more than 2.5 days) (Figure 7C). **4** adduct formation was time dependent, with increasing adducts formed with increasing time of incubation, with 50% dsDNA stabilization being attained within 5 h (Figure 7D) similar to the result shown for **7** (Figure 3C). Therefore, for the **1** backbone, chain length does not correlate with adduct formation efficiency as observed with the **2** backbone.

In Vitro Transcription Studies Demonstrate the Sequence Specificity of Formaldehyde-Activated Anthracenediones. An in vitro transcription assay was used to obtain the preferred sequence of binding sites for each derivative. The assay is based on blocking the progression of RNA polymerase along dsDNA. *Escherichia coli* RNA polymerase moves along dsDNA and is blocked each time it encounters a drug occupied site, thereby building up a number of truncated

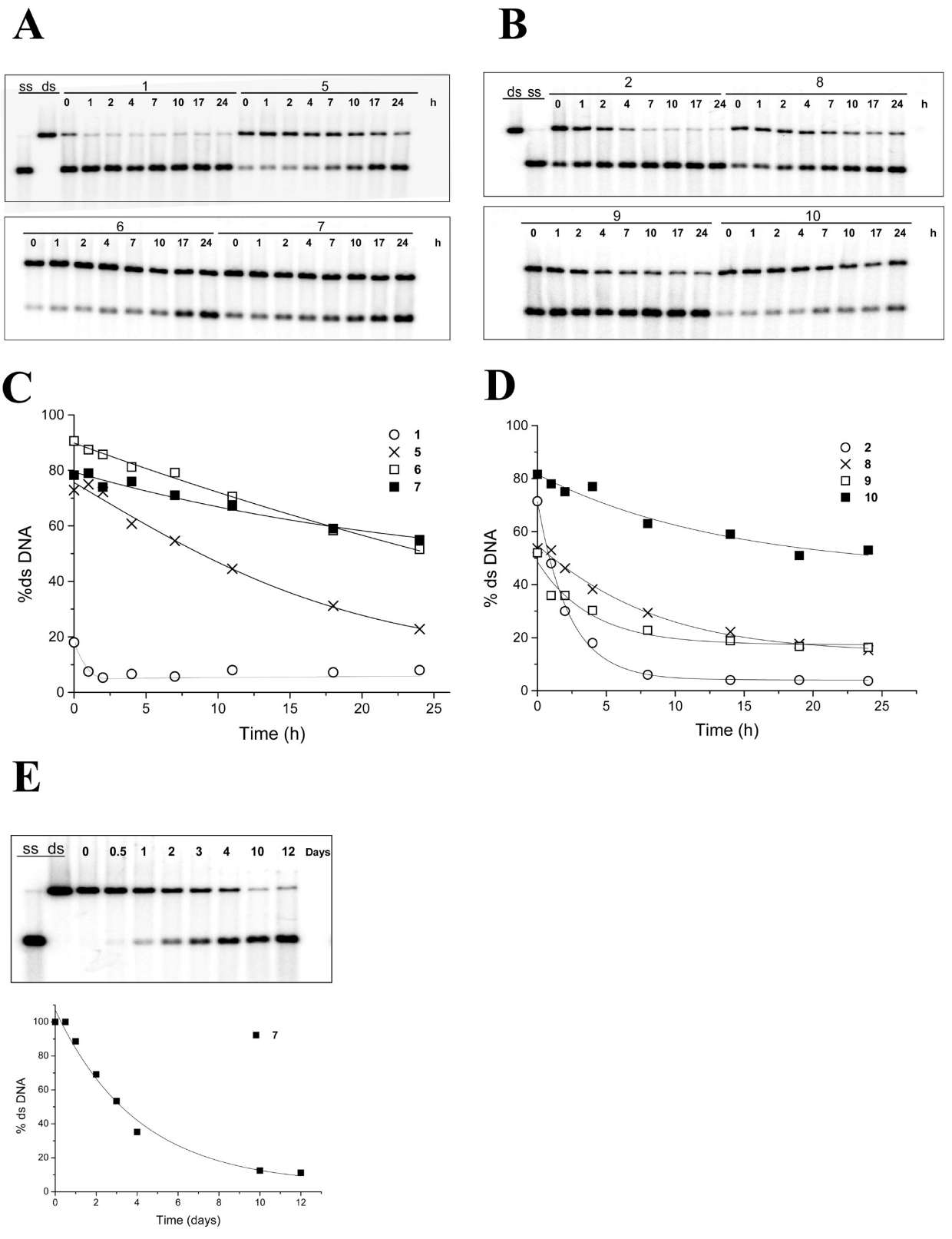

Figure 5. Stability of adducts induced by **1** and **2** derivatives. (A,B) **1** (36 μM), **5** (12 μM), **6** (8 μM), **7** (4 μM), **2** (5 μM), and **8**−**10** (40 μM each) were reacted with DNA in the presence of 2 mM formaldehyde at 37 °C for 16 h then subjected to a phenol/chloroform cleanup and left, as indicated, for time periods up to 24 h at 37 °C, then exposed to a second phenol/chloroform extraction and characterized after overnight electrophoresis. Control ssDNA is the unreacted DNA thermally denatured, while the dsDNA control was native dsDNA. (C) Quantitation of gel (A). The percentage of dsDNA stabilized for **1** (○), **5** (×), **6** (□), and **7** (■) reacted DNA samples was quantitated and expressed as a function of time. (D) Quantitation of gel (B). The percentage of dsDNA stabilized for **2** (○), **8** (×), **9** (□), and **10** (■) reacted DNA samples was quantitated and expressed as a function of time. (E) **7** (4 μM) was reacted with DNA in the presence of 2 mM formaldehyde at 37 °C for 16 h and then subjected to a phenol/chloroform cleanup and left, as indicated, for time periods up to 12 days at 37 °C. The percentage of dsDNA stabilized for **7**-reacted DNA samples was quantitated and expressed as a function of time.

Table 1. DNA Adduct Stability (In Vitro Crosslinking Assay)

compd	chain length	adduct half-life (h)[a]
1	NA	0.5[b]
4	2	2.3 ± 0.1
5	3	14 ± 0.4
6	4	30 ± 0.9
7	5	53 ± 7
2	2	2.3 ± 0.1
8	3	13 ± 0.1
9	4	16 ± 0.2
10	5	35 ± 0.1

[a] The adduct half-life is shown for each compound. Error values indicate the error of the exponential decay fit to the data. [b] This figure was taken from ref 24.

transcripts. The location of the drug binding sites can be obtained from the length of these truncated RNAs. When there are no DNA adducts, the RNA polymerase can move along the entire DNA template, generating 379 nucleotide full length transcripts.

Recently, it was established that formaldehyde-activated **2** generates DNA lesions which block the progression of RNA polymerase during transcription and cause drug-induced blockages at CpG and CpA dinucleotide sequences.[25] DNA adducts induced by formaldehyde-activated **1** and **2** derivatives were assessed using the in vitro transcription assay. A 512 bp fragment containing the *lac* UV5 promoter was reacted with each derivative in the presence of formaldehyde (Figure 8A). Each anthracenedione blocked RNA polymerase at similar sequences, indicating that all of these compounds have similar sequence specificity for adduct formation. The similarity of these discrete transcriptional blockages to those observed for **1** and **2** indicate that the sequence preference of all derivatives is CpG and CpA specific. The most intense blockages occurred at either CpG or CpA dinucleotides (Figure 8B,C,D; for sequence specificity histograms for all compounds see Supporting Information). Transcriptional blockages were also shown to increase with increasing concentrations of the drugs and with increasing reaction time (data not shown).

Molecular Modeling of DNA Adducts Induced by Formaldehyde-Activated Anthracenediones. Figure 9 shows **7** intercalated between the C_3 and G_4 bases of the hexanucleotide $d(ACCGGT)_2$ from the minor groove and the drug covalently bound through an aminal linkage to the N-2 atom of the G_5 residue on each strand. Although it was possible to form bis adducts with the N-2 atoms from both G_4 residues, the G_5 bis adducts gave lower energies. The terminal amine of **7** in the noncovalent intercalation complex is ideally positioned to form a covalent adduct with the G_5 residues on each strand. The modeling suggests that the formation of a G_5 cross-linked bis adduct causes very little disruption to the hexanucleotide structure. Alternatively, a cross-linked bis adduct with the G_4 residues introduces perturbations to the helix.

The modeling demonstrated that G_5 cross-linked bis adducts are also preferred for **1** derivatives **4**−**6**. However, the G_5 bis adduct formed with **4** induced noticeable deformation to the hexanucleotide structure. While it was possible to form G_5 bis adducts with **5** and **6** without significantly distorting the helix, it was noted that these adducts were less flexible than those formed with **7**. The reduced flexibility could reduce the ability of the helix to reform after random structural fluctuations that occur at 37 °C, thereby making the aminal linkages more susceptible to hydrolysis.

Growth Inhibition Induced by Formaldehyde-Activated Anthracenediones. The biological activity of each **1** derivative was evaluated in MCF-7 breast adenocarcinoma, PC-3 prostate, and HL60 acute promyelocytic leukemia cells using growth inhibition assays. As single agents, drug-induced growth inhibition generally decreased with increasing side-chain length (Table 2). The growth inhibition assays were also performed in the presence of **3** (as a formaldehyde-releasing prodrug) and CI values calculated to determine the types of drug interactions. Generally, there was a tendency for CI values to decrease as side-chain length increased for the compound series **4**−**7**. This trend was most evident in the HL60 cells for the combination with **3**, where **4** demonstrated antagonism, **5** demonstrated slight antagonism, **6** showed slight synergism, and **7** displayed moderate synergism. In PC-3 cells, the same trend was observed in combination experiments where **6** displayed synergism, however, only moderate synergism was observed for **7**. The trend was least obvious in MCF-7 cells, where increasing side chain length only led to a slight decrease in CI values. It should be noted that because IC_{50} values generally increased with increasing side-chain length, the molar excesses of **3** resulted in comparatively higher **3** concentrations used. However, CI calculations take into account the intrinsic contribution of each drug to growth inhibitory effects.

Discussion

It has previously been shown that formaldehyde is involved in the activation of **1**, which can subsequently bind covalently to DNA, forming adducts at CpG sequences of duplex DNA.[11,12] These adducts are formed by a linkage between the secondary amino portion of the side arm of **1** and the N-2 of guanine.[17] The potential involvement of a primary amino group instead of a secondary amino group to create a covalent N−C−N aminal linkage to the N-2 of guanine was investigated using **2**.[18,19] **2**, which bears a primary amino group in each of its side chains, was able to form DNA adducts much more effectively than **1**, forming a covalent linkage at CpG sequences with DNA caused by reaction with at least one accessible guanine at the N-2 position.[24] **2**−DNA adducts are more stable than **1**−DNA adducts, yet both half-lives are less than 2 h, indicating that the adducts are unstable.[24] On the basis of an energy-minimized structure of both the intercalated and covalently bound **1**,[17] it was suggested that the extension of the side arms of **2** may permit covalent linkage to both DNA strands, thereby creating a more reactive and possibly more stable adduct. The same underlying principle was also applied to derivatives based on a **1** backbone. The capacity of these derivatives to bind covalently to DNA and to form stable DNA adducts was then investigated, together with their DNA sequence specificity and growth inhibitory effects.

Chemistry. The synthesis of analogues **4**−**7** and **8**−**10** were from the respective difluoro anthracenedione precursors, **12** or **16**. The difluoro anthracenediones **12** and **16** were synthesized via a Friedel−Crafts bis-cycloacylation from the corresponding anhydrides **11** and **13**. The difluoro anthracenediones **12** and **16** were then reacted under S_NAr conditions, with the appropriate methylenediamine, to yield the desired substituted anthracenediones **4**−**7** and **8**−**10** (Scheme 1). This methodology was established by Krapcho et al.[28,29]

Formaldehyde-Activated Anthracenediones Form Stable Covalent Drug−DNA Adducts. All formaldehyde-activated anthracenedione derivatives were able to stabilize dsDNA by forming DNA adducts that were detectable using the in vitro cross-linking assay. The formation of these adducts was

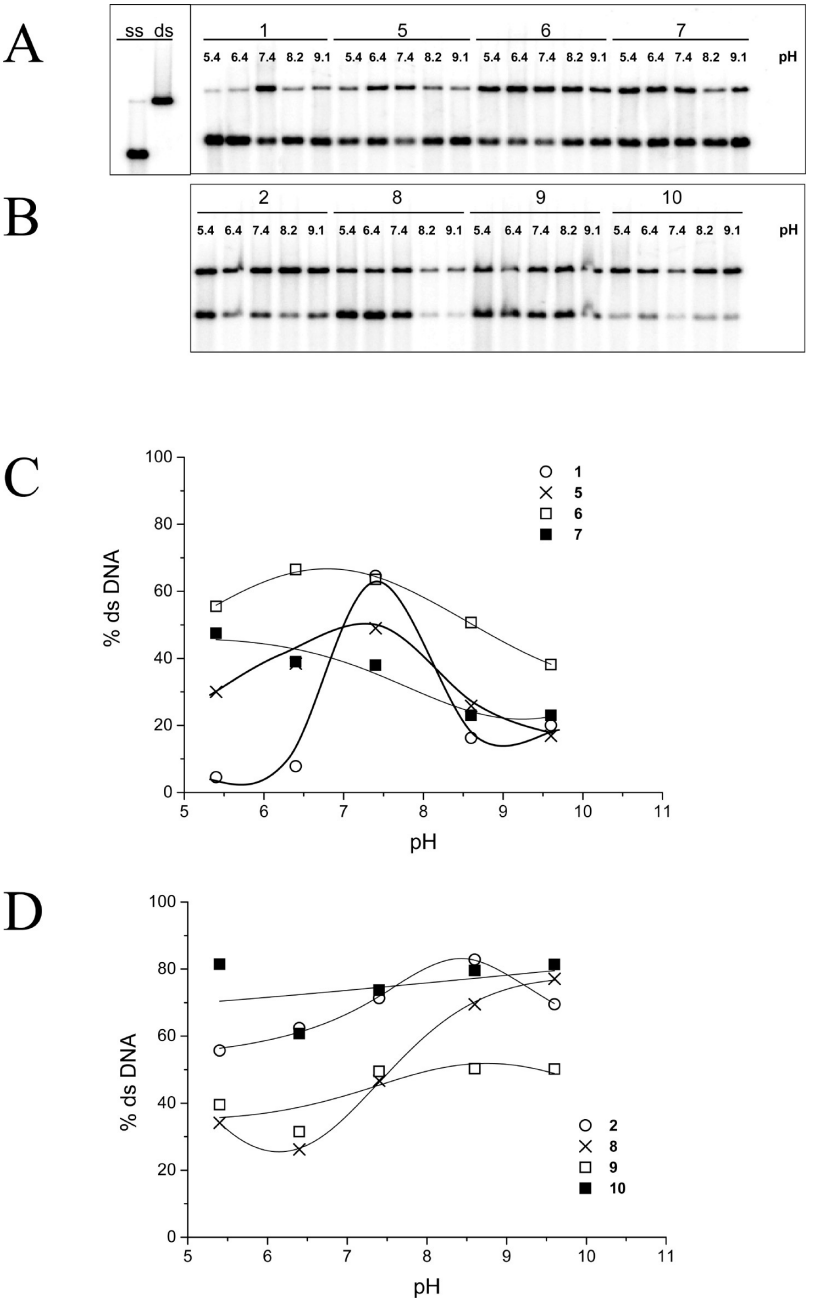

Figure 6. pH dependence of adduct formation displayed by **1** and **2** derivatives. (A,B) **1** (40 μM), **5** (12 μM), **6** (8 μM), **7** (4 μM), **2** (5 μM), **8** (50 μM), **9** (50 μM), and **10** (40 μM) were incubated with 2 mM formaldehyde at 37 °C for 16 h in PBS adjusted to various pHs ranging from 5.4 to 9.6 (as indicated). (C) Quantitation of gel (A). The percentage of dsDNA stabilized for **1** (○), **5** (×), **6** (□), and **7** (■) reacted DNA samples was quantitated and expressed as a function of pH. (D) Quantitation of gel (B). The percentage of dsDNA stabilized for **2** (○), **8** (×), **9** (□), and **10** (■) reacted DNA samples was quantitated and expressed as a function of pH.

dependent on drug and formaldehyde concentration, with **1** analogues bearing extended side-chains forming adducts at low concentrations compared to **1**. In contrast, **2** formed more adducts at low concentrations relative to its analogues with extended side-chains (Figure 2). **4**−**7** and **2** all formed adducts to a similar degree, indicating that the side-chain length is not a major determinant in adduct formation but rather the presence of a primary amino group is the primary determinant. The primary amino group is known to be considerably more reactive than a secondary amino group, thus providing a greater concentration of reactive drug−Schiff base precursor. Moreover, this drug−Schiff base complex is also more stable than secondary amino groups, therefore providing greater potential for reaction with DNA. The presence of the primary amine was previously shown to be crucial in the formation of **2**−DNA adducts in the presence of formaldehyde as BBR2378 (a dimethyl N-substituted analogue of **2**) was unable to stabilize dsDNA in vitro nor form monoadducts in the presence of formaldehyde.[25] The introduction of the pyridine ring for the dihydroxyphenylene moiety of the **1** chromophore has been associated with a compromised DNA binding affinity.[30] This is consistent with the results presented in Figure 2: each compound with a **2** backbone is less effective than the corresponding **1**-based compound.

For all the derivatives, the formation of adducts was also dependent upon the level of formaldehyde (Figure 4). Also,

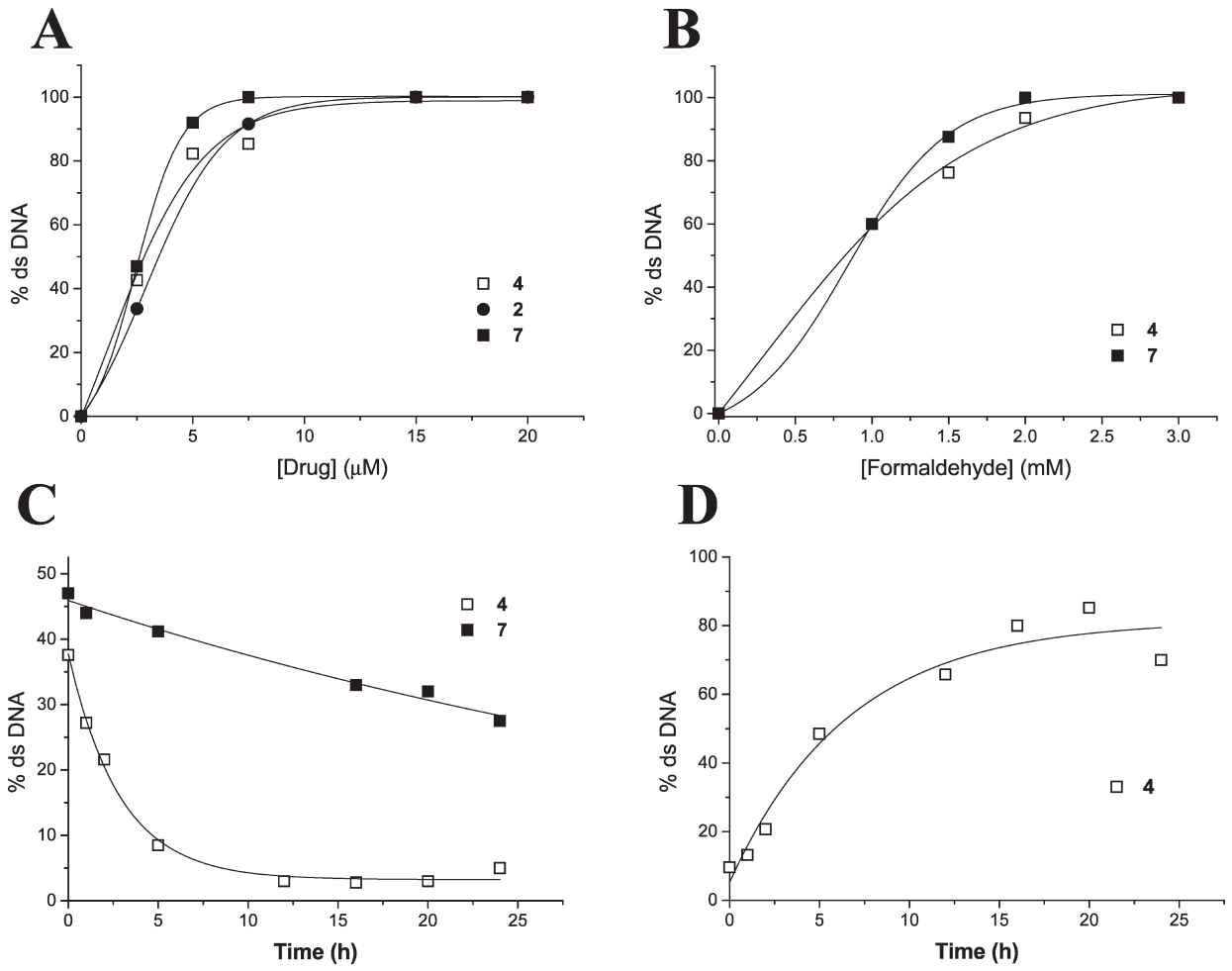

Figure 7. Formation of **4**−DNA adducts. (A) Concentration dependence of adduct formation displayed by **4**, compared to **7** and **2**. (B) Formaldehyde concentration dependence of adduct formation displayed by **4** and **7**. (C) Stability of adducts induced by **4** and **7**. (D) Time dependence of adduct formation displayed by **4**.

there was no adduct formation in the absence of formaldehyde, confirming a vital role for formaldehyde in the formation of drug−DNA adducts. Following nucleophilic attack by an amine within a side-chain of the drug, formaldehyde forms a reactive Schiff base intermediate, providing a likely binding site to DNA. The nature of the **2**−DNA covalent linkage was shown to be a methylene bridge formed by formaldehyde.[25] Given the structural similarities shared by all derivatives, and by analogy with **2**, this was also expected to be the nature of the covalent linkage created between the derivatives and DNA. This was indeed confirmed by mass spectrometric analysis of the **8**−DNA adduct (data not shown).

1 can exist as different ionic types and conformations in aqueous solutions and a change in pH (and temperature) can cause an equilibrium shift between the forms of the **1** molecule. However, it has been established that **1** exists predominantly in one molecular form in neutral aqueous solutions.[31] A change in the pH induces a conformational change in **1** where the nitrogen atom in the lateral chain forms a hydrogen bond with the deprotonated oxygen atom of the hydroxyl group at the tenth position. This may explain the strong pH-dependence of formaldehyde-activated **1**−DNA adduct formation (Figure 6). Moreover, while the secondary amino group of **1** could conceivably form an unstable aminal with formaldehyde, it cannot form an imine. This inability to form an imine may explain the different behavior of **1** with variation of pH (Figure 6). This also may explain the comparative pH-independent response of the derivatives.

A highlight of the present study is the outstanding stability exhibited by both **7** and **10** drug−DNA adducts relative to the parent compounds. As anticipated, all **1**−DNA adducts were lost in the first hour (Figure 5C), while **2**−DNA adducts were more stable but were still lost relatively quickly (in 120 min, Figure 5D). Strikingly, adduct stability increased with increasing side chain length. **7** formed the most stable adducts, with ~100-fold enhanced stability compared to the **1**−DNA lesion (Table 1).

For a conventional DNA interstrand cross-linking agent such as cisplatin, the two DNA strands are covalently joined together by the drug, thereby generating a stable cross-link. This is also postulated to be the case for stable **7** adducts where aminal linkages to the N-2 of guanine on both side chains could be accommodated to form a cross-link within steric constraints, as anticipated by initial molecular modeling studies[17] and shown to be feasible in the molecular model of a **7**−DNA adduct (Figure 9). Adducts formed by other formaldehyde activated derivatives previously studied act as monoadducts where the adduct is covalently bound via a single methylene bridge (provided by formaldehyde) to a single DNA strand and presumably complemented by hydrogen bonds to the opposite DNA strand with the chromophore intercalated

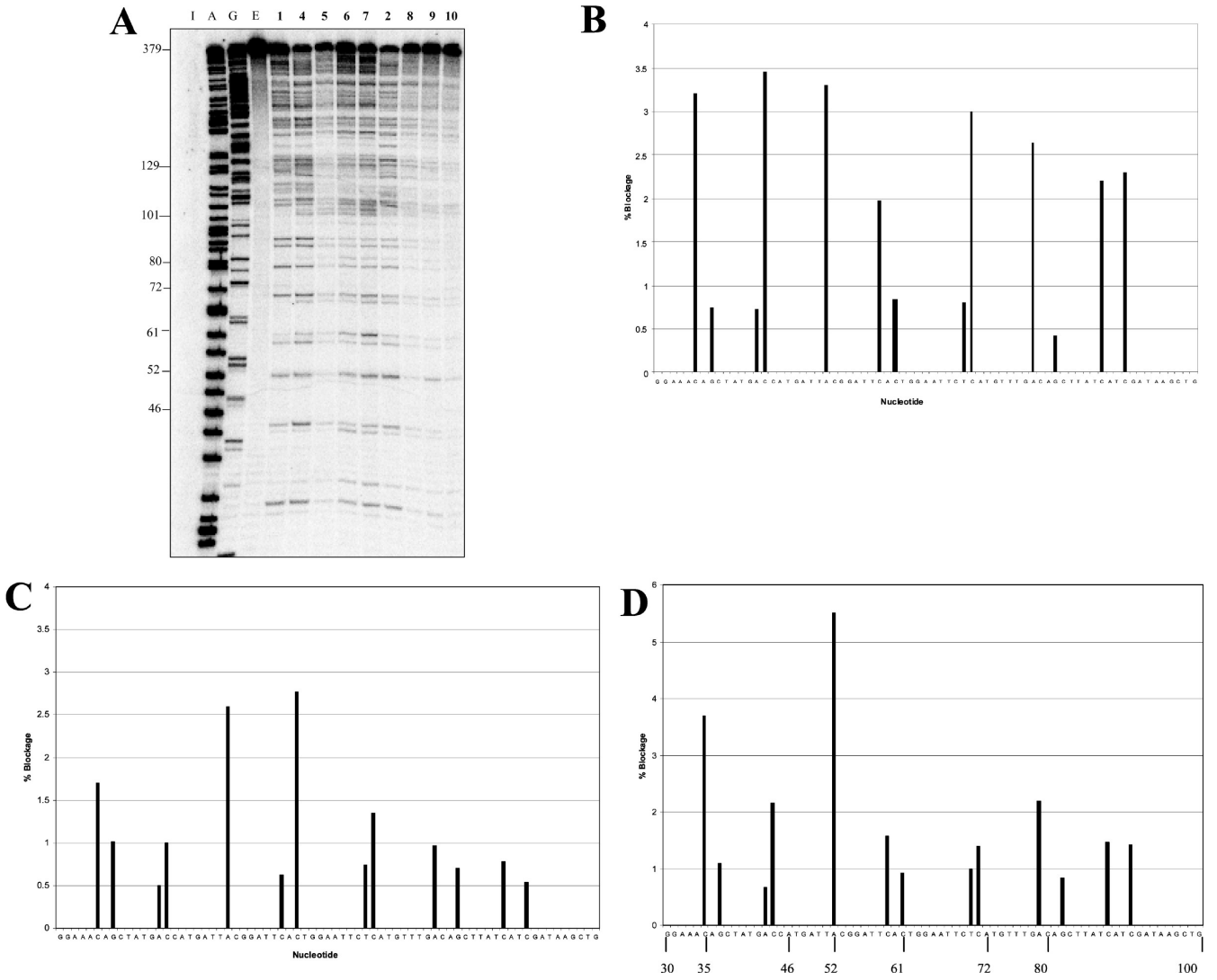

Figure 8. Sequence specificity of **1** and **2** derivatives. (A) In vitro transcription assay demonstrating the sequence specificity of **1** and **2** derivatives at 4 h. Drug-reacted samples were subjected to a transcription stop assay. Following initiation from the lac UV5 promoter, the transcription complex was elongated for 5 min and then terminated. Lanes I and E are controls representing an initiated complex that has not been elongated and extension of this complex to generate the full length transcript, respectively. Lanes A and G are sequencing lanes which were obtained using 3′-*O*-methoxy-ATP or 3′-*O*-methoxy-GTP during elongation, respectively. The length of selected transcripts is indicated at the left of the phosphorimage. (B) The sequence selectivity of formaldehyde-activated **4**, (C) **7**, and (D) **2**. The % transcriptional blockage of each transcript in the drug lanes from nucleotide 30 to 100 in (A) were quantitated and are expressed as a function of the sequence of a portion of the 512 bp DNA fragment. The sequence of the nontemplate DNA strand is shown. Transcriptional blockages less than an arbitrary value of 0.2% have been omitted. The numbers at the bottom of histogram (D) indicate the length of transcripts represented at the left of the phosphorimage in (A).

between neighboring base pairs, accounting for the relative instability.[13]

Formaldehyde-Activated Anthracenedione Derivatives Form CpG- and CpA-Specific Adducts. DNA−ligand interactions are of crucial importance to biological processes such as DNA replication and transcription. It has become clear that DNA sequence specificity is an essential factor contributing to the cytotoxic influence of numerous antitumor agents.[32−34] Recently, the DNA sequence involved in the formaldehyde-mediated **2**−DNA adducts was characterized, and formaldehyde activated **2** was shown to form CpG and CpA specific adducts,[25] revealing a prominent resemblance to **1** in sequence selectivity.[11,25] In vitro transcription studies showed that each derivative produced DNA lesions capable of blocking the progression of RNA polymerase (Figure 8), resulting in an overall inhibition of transcription and the generation of truncated transcripts. Relatively high levels of transcriptional blockages were produced by most **1** derivatives within the first 4 h (Figure 8A) and increased after 24 h (data not shown). **2** derivatives did not produce high levels of transcriptional blockages (Figure 8A) because a much higher concentration was required for adduct formation. Both **4**- and **2**-generated lesions caused the same level of transcriptional blockages, consistent with the same level of adducts caused by the two compounds in the in vitro cross-linking assay.

A distinguishing aspect of the transcriptional blockages is that they all occurred in a sequence-dependent manner (Figure 8A). The strong similarity of these distinct transcriptional blockages to those observed for **1** and **2** indicate that the sequence preference of all the derivatives is CpG and CpA specific.[11,25] This was confirmed by quantitation of truncated transcripts (Figure 8B,C,D) where the most intense blockage sites for derivatives was at CpG and CpA sequences (the full data set is available as Supporting

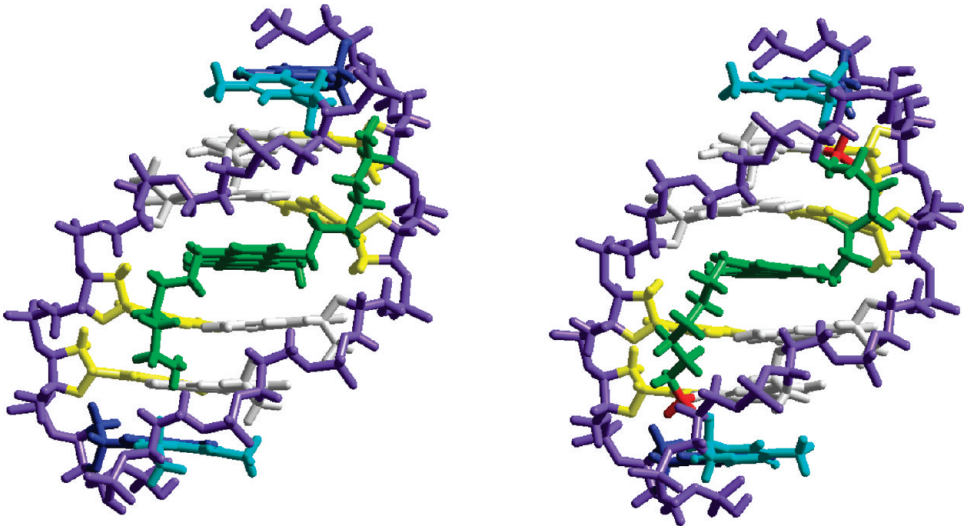

Figure 9. Modeling of **7** intercalated into DNA compared to the covalently bound form. **7** intercalated between the C_3 and G_4 bases of the hexanucleotide d(ACCGGT)$_2$ from the minor groove (left-hand side) and the compound covalently bound through aminal linkages to the N-2 atom of the G_5 residue on each strand. **7** is shown in green, and the additional carbon resulting from formaldehyde activation is red. The adenine residues are shown in blue, the thymine residues in cyan, the guanine residues in white, and the cytosine residues in yellow. The DNA backbones are shown in purple.

Table 2. Growth Inhibition Induced by **1** Derivatives As Single Agents and in Combination with a Formaldehyde-Releasing Prodrug[a]

	MCF-7		
compd	IC_{50} (nM)	IC_{50} + **3** (nM)[d]	CI
1	71 ± 30	240 ± 120	3.56
4	190 ± 88	190 ± 100	1.16
5	2900 ± 2300	990 ± 520	1.27
6	12000 ± 3000	840 ± 110	0.86
7	6700 ± 600	900 ± 320	0.98
3	107 ± 7[c]	N/A	
	PC-3		
compd	IC_{50} (nM)	IC_{50} + **3** (nM)[d]	CI
1	680 ± 160	400 ± 160	0.76
4	590 ± 480	480 ± 320	1.03
5	6300[b]	1200 ± 280	0.73
6	10800[b]	730 ± 120	0.39
7	4800 ± 1000	1290 ± 30	0.85
3	230 ± 40[c]		
	HL60		
compd	IC_{50} (nM)	IC_{50} + **3** (nM)[e]	CI
1	7 ± 2	11 ± 6	1.74
4	9 ± 3	17 ± 10	1.82
5	260 ± 110	205 ± 10	1.17
6	1700 ± 190	360[b]	0.87
7	3800 ± 1100	350 ± 60	0.73
3	22 ± 13[c]		

[a] IC_{50} values are shown as the concentration as which 50% of cells survived. The interaction of the drugs in combination was evaluated from IC_{50} values by calculating the combination index. The combination index (CI) was calculated as described in the Experimental Section. Two experiments were performed independently in quadruplicate. Data is shown as mean ± SD. [b] Denotes data from a single experiment performed in quadruplicate. [c] Denotes that the concentration is μM. [d] A 100-fold molar excess of **3** was used. [e] A 40-fold molar excess of **3** was used.

Information). Because **1** has been found to intercalate preferentially at CG and CA sites in DNA,[35] it therefore appears that this enables subsequent activation by formaldehyde at these sites, leading to the covalent binding to adjacent nucleotides on the DNA where a reactive site is available. This also suggests that the sequence specificity of intercalation by the derivatives

Scheme 1. Synthesis of the **1**-Derived **4**−**7** and the **2**-Derived **8**−**10** Analogues[a]

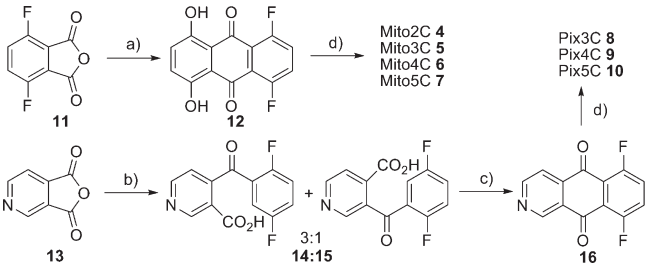

[a] Reagents and conditions: (a) hydroquinone, $AlCl_3$, NaCl, 200 °C, 5 h, 60%; (b) 1,4-difluorobenzene, $AlCl_3$, ⇅, 20 h, 84%; (c) oleum (30% SO_3) 135 °C, 3 h, 86%; (d) 4 equiv $NH_2(CH_2)_nNH_2$, THF, 50 °C, 20 h.

may be similar to **1**. In fact, the guanine base of DNA is well-known to contain reactive and accessible sites.[36−38] As other formaldehyde-activated drugs like **1**, doxorubicin and **2** bind to guanine via the exocyclic N-2 amino group,[13,17,25] it is likely that all of the formaldehyde-activated derivatives bind covalently via a methylene group to the DNA through the exocyclic N-2 amino group of guanine, leading to the formation of N−C−N aminal linkages.

In addition to the importance of recognizing appropriate DNA sequences in overcoming the problem of generalized toxicity of a drug, the CpG recognition by the formaldehyde-activated derivatives is significant because this dinucleotide holds a distinctive function in the mammalian genome. The possibility of finding any dinucleotide in a given DNA sequence is 1/16 (about 6%). In humans, however, the measured frequency of the CpG dinucleotide is very low, an event referred to as CG suppression. Despite this, some genomic regions contain a high frequency of CpG dinucleotide known as CpG islands, which typically occur in clusters within 300−3000 bp regions. These are frequently associated with the promoter region of many genes (in about 70% of human promoters),[39−42] making them an excellent selective target for anthracenedione derivative−DNA adducts outlined in this work.

Molecular Modeling Studies. In an effort to explain the exceptional stability of **7**−DNA adducts compared to adducts formed with other derivatives, modeling studies were undertaken. In the energy minimized model (Figure 9), it is apparent that the intercalation optimum for **7** is symmetrical, which contrasts with the earlier study with the parent compound **1**.[17] Similar models of **1** intercalated between the C_3 and G_4 bases of the hexanucleotide $d(ACCGGT)_2$ could not produce a symmetrical intercalation optimum. An obvious explanation for the increased stability of **7**−DNA adducts is the potential for intercalated **7** to form aminal linkages at two accessible guanine N-2 positions with minimal distortion to the helix. Furthermore, with the less stable drug−DNA adducts, the aminal bonds would be more readily hydrolyzed in a molten DNA state because of the contribution of base-pairing to the electronic state of the guanine ring. Cytosine residues lend electron density to the guanine ring through multiple hydrogen bonds, contributing to the reactivity of the unmodified guanine N-2. Formation of an aminal adduct at N-2 would make N-2 withdraw electrons less strongly from the adjacent aminal carbon, making the aminal carbon less susceptible to nucleophilic attack. In this way, the longer cross-link induced by **7** may contribute to chemical stability by contributing to the DNA duplex thermostability

Interactions with the Formaldehyde-Releasing Prodrug 3. Significant synergism was demonstrated in cultured cells treated with a combination of formaldehyde releasing prodrugs and doxorubicin.[19,43] However, this synergy is not observed for **1** in combination with formaldehyde-releasing prodrugs (unpublished results) and this is most likely due to the instability of DNA adducts. Derivatives **4**−**7** form increasingly stable DNA adducts following formaldehyde activation in vitro (Figure 5 and Table 1), and this generally appeared to be associated with decreasing CI values (Table 2). **4**, which achieved a similar level of reactivity as **7** (Figure 7) but formed much less stable DNA adducts, did not exhibit synergy in combination with **3** in any of the cell lines studied. This may reflect the importance of inducing stable DNA adducts which can maximize DNA damage and potentially impair crucial cellular processes such as DNA replication and transcription. However, in PC-3 cells, **7** (that formed the most stable DNA adducts) did not conform to the general trend. This may be due to our observation that increased side chain length appears to favor lysosome versus nuclear localization in cell lines with extensive lysosomal networks (unpublished results), and this is a subject of future investigations.

Another factor that might be contributing to the synergy displayed by some of the derivatives with **3** is the esterase hydrolysis of **3** and the release of the cellular histone deacetylase inhibitor butyric acid.[44] Histone deacetylase (HDAC) inhibitors have now emerged as a new class of potential anticancer agents for the treatment of solid and hematological malignancies.[45] HDAC inhibitors change the expression of genes by causing an increase in histone acetylation, thus regulating chromatin structure and transcription.[46,47] Inhibitors such as suberoylanilide hydroxamic acid (SAHA) have been tested in combination with a variety of conventional cytotoxic chemotherapeutics.[48] It is well documented that cultured cells pretreated with HDAC inhibitors display enhanced activity of DNA damaging agents.[49] However, given our knowledge of anthracenedione activation and observation of doxorubicin/**3** interactions,[43] the formaldehyde contribution to the observed synergy is more likely.

A problem with the development of new anticancer compounds based on traditional chemotherapeutic compounds, such as the anthracyclines and anthracenediones, is their limited selectivity for tumor vs nontumor cells. A potential solution can now be presented with respect to the new types of compounds outlined in the present study—an inherent dependence on formaldehyde for biological activity means that tumor-targeted formaldehyde is a potential treatment strategy in conjunction with anthracenedione therapy. Another key problem in the development of anticancer drugs is the large gap between promising findings in preclinical in vitro models and the results of clinical trials. Drug combinations that displayed evidence of synergy in this study will next be subjected to rigorous analysis, particularly with respect to their anticancer activity in clonogenic assays in vitro and effects on tumors in vivo.

Experimental Section

Materials. **3** was synthesized and provided by Professor Abraham Nudelman, Ramat-Gan University, Israel. Formaldehyde solution (40% w/v) and chloroform were purchased from Merck (BDH). Calf thymus DNA was obtained from Worthington Biochemical Corporation. Tris-saturated ultrapure phenol and 1 Kb plus DNA marker were purchased from Invitrogen. Ultrapure dNTPs, 3′-*O*-methyl NTPs, GpA dinucleotide, [α-^{32}P] dATP, [α-^{32}P] dCTP, [α-^{32}P] UTP (3000 Ci/mmol), RNAguard RNase inhibitor, and ProbeQuant G-50 columns were all from GE Healthcare. TEMED and the two restriction enzymes *Hind*III and *Pvu*II were purchased from Promega. *E. coli* RNA polymerase and glycogen were both obtained from Roche. The Klenow fragment of DNA polymerase I and BSA were obtained from New England Biolabs. Acrylamide:bisacrylamide solution was purchased from Amresco and molecular biology grade urea from MP Biomedicals. Formamide, heparin, and the tetrazolium salt MTT [3-(4,5-dimethylthiazol-2-yl)-2,5-diphenyltetrazolium bromide] were all obtained from Sigma Chemical Co. A Maxi Plasmid purification kit was purchased from Qiagen and DTT and ammonium persulfate were both from Bio-Rad.

Methods. Drug Preparation for Biological Assays. All drugs were dissolved in Milli-Q water (distilled water purified on a Millipore Q system) to a final concentration of between 0.5 and 2 mM and subsequently stored at −20 °C. On the day of each experiment, the precise concentrations of the drugs were determined spectrophotometrically on a Cary 118C spectrophotometer using $\varepsilon = 19200\ M^{-1}cm^{-1}$ at 608 nm for **1** and its analogues and $\varepsilon = 16500\ M^{-1}cm^{-1}$ at 641 nm for **2** and its derivatives. **3** was diluted in DMSO in glass vials using glass syringes. Formaldehyde and **3** solutions were freshly prepared at the time of each experiment.

DNA Source and End-Labeling. The plasmid pCC1[27] was initially restriction digested with *Hind*III at 37 °C for 2 h and subsequently end-labeled at the 5′-overhang with [α^{32}P] dCTP using the Klenow fragment of DNA polymerase I. A G-50 ProbeQuant chromatography column was then used to remove unincorporated label from the labeled DNA fragment. The sample was subsequently subjected to phenol/chloroform extraction, ethanol precipitation, and resuspension in 1× TE (10 mM Tris, 1 mM EDTA, pH 8.0). The final DNA concentration was adjusted to 400 μM_{bp} by the addition of sonicated calf thymus DNA.

In Vitro Cross-Linking Assay. The end-labeled DNA was used for in vitro DNA binding reactions where covalently bound drug−DNA adducts were formed. Each reaction mixture typically contained 25 μM_{bp} end-labeled DNA, formaldehyde, and the anthracenedione of interest in phosphate-buffered saline, pH 7.0 (PBS), and were reacted at 37 °C for the desired amount of time. Noncovalently bound drug was removed from the reaction mixture by two extractions with an equal volume of Tris-saturated phenol followed by a single extraction with an

equal volume of chloroform. Drug-reacted DNA samples were then precipitated with a mixture containing ethanol, sodium acetate, and glycogen as a carrier to improve recovery. Sample pellets were subsequently resuspended in 1× TE buffer and denatured in two volumes of loading dye (90% formamide, 10 mM EDTA, 0.1% bromophenol blue, 0.1% xylene cyanol) at 52 °C (or a range of temperatures where the denaturation temperature was determined) for 5 min. Samples were subjected to electrophoresis through 0.8% agarose gels overnight at 40 V in 1× TAE (Tris-acetate EDTA) buffer. Gels were vacuum-dried in a Bio-Rad model 583 gel drier and subsequently exposed to a phosphor screen for 4 h. A Typhoon Trio PhosphorImager (GE Healthcare) was used to generate a phosphorimage of the dried gel, and ImageQuant software was used for analysis and quantitation.

Experiments assessing drug−DNA adduct stability were performed in an identical manner, however, each sample was subjected to an additional extraction procedure following incubation at 37 °C for defined time periods. The additional step utilized an extraction once with phenol, once with chloroform, and a final ethanol precipitation. Resuspended DNA samples were subjected to electrophoresis as described above.

In Vitro Transcription. Plasmid pCC1 was subjected to restriction digestion with *Pvu*II and *Hind*III for 2 h at 37 °C to liberate a 512 bp fragment containing the *lac* UV5 promoter.[27,50] The 512 bp restriction fragment was subsequently isolated using electrophoresis followed by electroelution as previously described.[51] The DNA fragment was finally purified by phenol/chloroform extraction, ethanol precipitation, and resuspension in 1× TE buffer in preparation for drug reaction.

The 512 bp DNA fragment (25 μMbp) was reacted with the drug of interest in the presence of formaldehyde in PBS (pH 7.0) at 37 °C for defined time periods. Drug-reacted DNA samples were then ethanol precipitated and resuspended in 1× TC (transcription buffer: 40 mM Tris pH 8.0, 100 mM KCl, 3 mM $MgCl_2$, and 0.1 mM EDTA). Each sample was subsequently incubated with a transcription mixture containing 0.025 U/μL *E. coli* RNA polymerase, 10 mM DTT, 125 μg/mL BSA, and 2 U/μL RNAguard RNase inhibitor in 1× TC buffer for 15 min at 37 °C. Heparin (400 μg/mL) was then added for 5 min to remove RNA polymerase from nonspecific binding sites on the DNA. An initiation mixture containing 200 μM GpA, 5 μM ATP, 5 μM GTP, and [α^{32}P] UTP in TC was then added to each sample again for 5 min at 37 °C. Transcripts were allowed to elongate by the subsequent addition of an elongation mixture containing 6 mM of each NTP and 1.2 mM KCl in 1× TC for 5 min at 37 °C. Transcription was terminated by the addition of an equal volume of loading/termination buffer (9 M urea, 10% sucrose, 40 mM EDTA, 0.1% xylene cyanol, and 0.1% bromophenol blue in 2 × TBE). All transcription samples were denatured at 90 °C for 5 min and immediately quenched on ice.

Sequencing of the RNA transcripts was achieved by incubating an unreacted batch of the 512 bp DNA fragment with the transcription mixture as described above. Samples were then allowed to elongate in the presence of 90 μM 3′-*O*-methoxy-ATP (or 3′-*O*-methoxy-GTP), 10 μM ATP (or GTP), 2 mM CTP, GTP (or ATP), UTP, and 400 mM KCl at 37 °C for 5 min. Reactions were terminated by the addition of an equal volume of loading/termination buffer, denatured at 90 °C for 5 min, and quenched on ice.

RNA drug-induced blocked transcripts were separated on a 12% acrylamide denaturing gel (19:1 acrylamide:bisacrylamide containing 7 M urea). The high resolution sequencing gel was prepared in 1× TBE buffer and subjected to pre-electrophoresis at 1800 V for 1−2 h. Denatured samples were loaded onto the gel and electrophoresed at 2000 V for approximately 2 h. The gel was then fixed with 10% acetic acid/10% MeOH, dried on a Bio-Rad gel drier, and exposed to a phosphor screen for 4 h. Phosphorimaging analysis and quantitation were performed as described for the in vitro cross-linking assay.

Molecular Modeling. Molecular modeling was carried out using HyperChem Release 7.5 Hypercube Inc. Point charges for the **1** derivatives and the various covalent adducts were based on AM1 optimizations. The duplex B-type hexanucleotide $d(ACCGGT)_2$ was generated from the nucleic acid database and the **1** derivative manually intercalated between the C_3 and G_4 bases. The drug−oligonucleotide complex was then minimized in vacuo using the Amber 99 force field and a Polak−Ribiere conjugant-gradient algorithm with a 5×10^{-5} kcal/(Å mol) convergence criteria. Covalent adducts, involving the N-2 of G_4 and G_5, were prepared and energy minimized in a similar fashion.

Cell Culture and Growth Inhibition Assay. MCF-7 breast adenocarcinoma cells (obtained from Dr Rosanna Supino, Istituto Nazionale Tumori, Milano, Italy), PC-3 prostate cancer cells (obtained from Dr Carleen Cullinane, Peter McCallum Cancer Institute, Melbourne, Australia), and HL60 promyelocytic leukemia cells (purchased from ATCC, VA, USA) were maintained in RPMI 1640 media (JRH Biosciences) supplemented with 10% fetal calf serum (Trace Scientific) at 37 °C in a humidified atmosphere with 5% CO_2.

Cells were seeded at a density of 4×10^3 cells/well (MCF-7 and PC-3) or 10^4 cells/well (HL60) into individual 96-well plates in 100 μL of complete media (RPMI 1640 with 10% FCS) and incubated overnight at 37 °C with 5% CO_2. The following day, a serial dilution of drugs was prepared and 50 μL/well of each drug was added in quadruplicate. Drug treatment consisted of serial dilutions of one anthracenedione, **3**, or a combination of both anthracenedione and prodrug. For single drug treatments, 50 μL of complete media was added to the wells to adjust the volume to 200 μL/well. For 4 h treatments (MCF-7 and PC-3), compounds were removed after 4 h and 200 μL fresh media replaced. After 72 h, 100 μL of the tetrazolium salt MTT dissolved in PBS (1 mg/mL and filtered through a 0.22 μm Millipore filter) was added to each well containing MCF-7 or PC-3 cells for 3−4 h at 37 °C. Overlying media was then removed by aspiration, and 100 μL/well of DMSO was added to solubilize the formazan (metabolized MTT). A Molecular Devices Spectra Max 250 microplate reader was used to measure the absorbance at 570 nm. HL60 cell growth inhibition was determined by MTS metabolism. MTS (Promega, WI, USA) and phenazine methosulfate (PMS) (Sigma, MO, USA) were each dissolved in PBS at a concentration of 1.6 mg/mL and sterile filtered. MTS and PMS were mixed at a ratio of 9:1 and 50 μL of this added to each well and the plates incubated for 3−4 h at 37 °C. Absorbance at 490 nm was determined in each well using a microplate reader.

Absorbance values were plotted against the log of the drug concentration, and sigmoidal fits were applied to yield IC_{50} values using Origin software (Microcal, MA, USA). IC_{50} values were determined as the concentration at which 50% of cells were metabolically active. Drug synergism was evaluated using the method of Chou and Talalay,[52] where a combination index[43] < 1 indicates synergy, a CI = 1 indicates additivity, and a CI > 1 indicates antagonism. The CI was calculated using the formula:

$$CI = (IC_{50}(\text{drug 1 in combination with drug 2})/IC_{50}(\text{drug 1 alone})) + (IC_{50}(\text{drug2 in combination with drug 1})/IC_{50}(\text{drug 2 alone}))$$

Chemistry. General Experimental. All nonaqueous reactions were performed in oven-dried glassware under an atmosphere of dry nitrogen, unless otherwise specified. All anhydrous solvents were purified using a Braun purification system. All other solvents were reagent grade. Petroleum ether describes a mixture of hexanes in the bp range 40−60 °C. Analytical thin-layer chromatography was performed on Merck silica gel $60F_{254}$ aluminum-backed plates and were visualized by fluorescence quenching under UV light. All NMR spectra were recorded on a Bruker Avance DRX 300 with the solvents indicated (^{1}H NMR at

300 MHz). Chemical shifts are reported in ppm on the scale, referenced to the appropriate solvent peak. HRESMS were recorded at the Australian National University Mass Spectrometry Facility using a Waters LCT Premier XE (ESI TOF mass spectrometer). LCMS was recorded on a Waters ZQ 3100 system using a Waters 2996 diode array detector. LCMS conditions used to assess purity of compounds were as follows: column, RP XBridge TM C18 5 μM 4.6 mm × 100 mm; injection volume, 10 μL; flow rate, 1.5 mL/min; gradient, 0−100% of B over 10 min, (solvent A, water; solvent B, AcCN, 0.1% formic acid). All compounds were ≥95% pure.

Experimental. 1,4-Dihydroxy-5,8-bis(2-(2-hydroxyethylamino)-ethylamino)anthracene-9,10-dione 1. Mitoxantrone hydrochloride **1** was obtained commercially from Sigma Chemical Co.

6,9-Bis(2-aminoethylamino)benzo[g]isoquinoline-5,10-dione dimaleate 2. Pixantrone dimaleate **2** was kindly provided by Cell Therapeutics Europe (Bresso, Italy).

3,6-Difluorophthalic Anhydride 11. 3,6-Difluorophthalic anhydride was prepared in an identical manner to that of Krapcho et al.[28]

1,4-Difluoro-5,8-dihydroxyanthracene-9,10-dione 12. The procedure followed was similar to that of Krapcho et al.[28] Hydroquinone (18.9 mmol) and 3,6-difluorophthalic anhydride **11** (18.0 mmol) were added portionwise to a stirred melt of $AlCl_3$ (198.0 mmol) and sodium chloride (72.0 mmol) at 200 °C under a nitrogen atmosphere. The mixture was stirred for 5 h at 200 °C. The solution was allowed to cool, and ice−water was added. Concentrated HCl (40 mL) was added, and the solution was stirred at room temperature for 3 h. The resulting precipitate was filtered off, washed with water, and dried in a vacuum oven to afford the dione **12** as a red solid (60%). ^{1}H NMR (DMSO) δ 7.87 (2H, m), 7.42 (2H, s).[28]

4-(2,5-Difluorobenzoyl)-nicotinic acid 14 and 3-(2,5-Difluorobenzoyl)-isonicotinic Acid 15 (3:1 Mixture). The procedure followed was similar to that of Krapcho et al.[29] Aluminum chloride (134.0 mmol) was added portionwise to a stirred solution of pyridine-3,4-dicarboxylic acid anhydride **13** (33.5 mmol) and 1,4-difluorobenzene (218.0 mmol) at 90 °C. The solution was refluxed for 24 h under a nitrogen atmosphere. The excess 1,4-difluorobenzene was distilled off and can be subsequently recycled. Ice−water (70 mL) was then added to the resulting residue, and concentrated HCl (6.3 mL) was added. The resulting precipitate was filtered off, washed with water, and dried in a vacuum oven to afford a white solid (84%) as a 3:1 mixture of 4-(2,5-difluorobenzoyl)-nicotinic acid **14** and 3-(2,5-difluorobenzoyl)-isonicotinic acid **15**, respectively. ^{1}H NMR (DMSO) δ 9.15 (s), 8.91 (d) 8.90 (d), 8.76 (s), 7.85 (d), 7.63−7.22 (m).[29]

6,9-Difluorobenzo[g]isoquinoline-5,10-dione 16. The procedure followed was similar to that of Krapcho et al.,[29] A 3:1 mixture of 4-(2,5-difluorobenzoyl)-nicotinic acid **14** and 3-(2,5-difluorobenzoyl)-isonicotinic acid **15** (11.4 mmol) in fuming H_2SO_4 (7.5 mL, 30% SO_3) was heated at 135 °C for 3 h. The mixture was allowed to cool, and ice−water was added. The solution was then neutralized by portionwise addition of solid $NaHCO_3$. The resulting precipitate was filtered off and washed with water. The solid was dried in a vacuum oven to obtain the dione **16**, a pale-yellow solid (86%). ^{1}H NMR (DMSO) δ 9.26 (1H, s), 9.06 (1H, dd), 7.91 (1H, d), 7.84−7.79 (2H, m).[29]

1,4-Bis(2-aminoethylamino)-5,8-dihydroxyanthracene-9,10-dione Dihydrochloride 4. A mixture of the difluoro dione **12** (75 mg, 0.27 mmol) and 1,2-diaminoethane (123 μL, 1.2 mmol) in THF (5 mL) was stirred at 50 °C for 20 h. The solution was cooled, and the precipitate was filtered off and washed with THF. The filtrate was concentrated in vacuo and the residue dried under high vacuum to remove excess amine. The residue was dissolved in MeOH (2 mL), and a solution of 1.25 N HCl in MeOH (1.62 mmol) was added. A sufficient volume of EtOAc was added, and a precipitate developed. The solid was filtered off and washed with EtOAc to give the dihydrochloride of **4** as a dark-blue solid (69 mg, 60%).[53] IR ν_{max} 2967, 1605, 1560, 1455, 1153, 1055, 791 cm^{-1}. HRESMS found: (M + H) 357.1559; $C_{18}H_{20}N_4O_4$ requires (M + H), 357.1563. ^{1}H NMR (DMSO) δ 10.40 (2H, t), 8.21 (6H, bs), 7.64 (2H, s), 7.17 (2H, s), 3.85−3.76 (4H, m), 3.08−3.00 (4H, m). LCMS: T_r = 4.24 min, 95% purity; m/z (%) = 357 (100), [M + H]$^+$ 296 (100).

1,4-Bis(3-aminopropylamino)-5,8-dihydroxyanthracene-9,10-dione Dimaleate 5. A mixture of the difluoro dione **12** (100 mg, 0.36 mmol) and 1,3-diaminopropane (302 μL, 3.6 mmol) in THF (5 mL) was stirred at 50 °C for 20 h. The solution was cooled, and the precipitate was filtered off and washed with THF. The filtrate was concentrated in vacuo and the residue dried under high vacuum to remove excess amine. The residue was dissolved in MeOH (2 mL), and a solution of maleic acid (126 mg, 1.1 mmol) in MeOH (1.5 mL) was added. A sufficient volume of EtOAc was added and a precipitate developed. The solid was filtered off, washing with EtOAc to afford the dimaleate of **5** as a dark-blue solid (101 mg, 45%).[53] IR ν_{max} 2953, 1606, 1555, 1454, 1353, 1205, 823 cm^{-1}. HRESMS found: (M + H) 385.1876; $C_{20}H_{24}N_4O_4$ requires (M + H), 385.1876. ^{1}H NMR (DMSO) δ 10.52 (2H, t), 7.69 (6H, bs), 7.56 (2H, s), 7.17 (2H, s), 6.01 (4H, s), 3.64−3.56 (4H, m), 2.92 (4H, t), 1.97−1.91 (4H, m). LCMS: T_r = 4.46 min, 95% purity; m/z (%) = 385 (100), [M + H]$^+$ 328 (60).

1,4-Bis(4-aminobutylamino)-5,8-dihydroxyanthracene-9,10-dione Dimaleate 6. A mixture of the difluoro dione **12** (75 mg, 0.27 mmol) and 1,4-diaminobutane (272 μL, 2.7 mmol) in THF (5 mL) was stirred at 50 °C for 20 h. The solution was cooled, and the precipitate was filtered off and washed with THF. The filtrate was concentrated in vacuo, and the residue dried under a stream of nitrogen to aid in removal of excess amine. The residue was dissolved in MeOH (2 mL), and a solution of maleic acid (94 mg, 0.81 mmol) in MeOH (1.5 mL) was added. A sufficient volume of EtOAc was added, and a precipitate developed. The solid was filtered off and washed with EtOAc to give the dimaleate of **6** as a dark-blue solid (78 mg, 45%).[53] IR ν_{max} 2942, 1607, 1556, 1449, 1202, 860 cm^{-1}. HRESMS found: (M + H) 413.2189; $C_{22}H_{28}N_4O_4$ requires (M + H), 413.2189. ^{1}H NMR (DMSO) δ 10.53 (2H, t), 7.66 (6H, bs), 7.56 (2H, s), 7.15 (2H, s), 6.01 (4H, s), 3.58−3.50 (4H, m), 2.90−2.82 (4H, m), 1.70−1.65 (8H, m). LCMS: T_r = 4.66 min, 95% purity; m/z (%) = 413 (90), [M + H]$^+$ 325 (100).

1,4-Bis(5-aminopentylamino)-5,8-dihydroxyanthracene-9,10-dione Dimaleate 7. A mixture of the difluoro dione **12** (75 mg, 0.27 mmol) and 1,5-diaminopentane (130 μL, 1.1 mmol) in THF (5 mL) was stirred at 50 °C for 20 h. The solution was cooled, and the precipitate was filtered off and washed with THF. The filtrate was concentrated in vacuo, and the residue dried under a stream of nitrogen to aid in removal of excess amine. The residue was dissolved in MeOH (2 mL), and a solution of maleic acid (142 mg, 0.93 mmol) in MeOH (1.5 mL) was added. A sufficient volume of EtOAc was added and a precipitate developed. The solid was filtered off and washed with EtOAc to give the dimaleate of **7** as a dark-blue solid (73 mg, 40%). IR ν_{max} 2940, 1609, 1562, 1456, 1353, 1200, 863 cm^{-1}. HRESMS found: (M + H) 441.2496; $C_{24}H_{32}N_4O_4$ requires (M + H), 441.2502. ^{1}H NMR (DMSO) δ 10.63 (2H, t), 7.55 (2H, s), 7.15 (2H, s), 6.00 (4H, s), 3.53−3.45 (4H, m), 2.95−2.78 (4H, m), 1.70−1.41 (12H, m). LCMS: T_r = 4.88 min, 95% purity; m/z (%) = 441 (35), [M + H]$^+$ 213 (100).

6,9-Bis(3-aminopropylamino)benzo[g]isoquinoline-5,10-dione Dimaleate 8. A mixture of the difluoro dione **16** (100 mg, 0.41 mmol) and 1,3-diaminopropane (340 μL, 4.1 mmol) in THF (5 mL) were stirred at 50 °C for 20 h. The solution was cooled, and the precipitate was filtered off and washed with THF. The filtrate was concentrated in vacuo and the residue dried under high vacuum to remove excess amine. The residue was dissolved in MeOH (2 mL), and a solution of maleic acid (142 mg, 1.2 mmol) in MeOH (1.5 mL) was added. A sufficient volume of EtOAc was added, and a precipitate developed. The solid was filtered off and washed with EtOAc to give the dimaleate of **8** a dark-blue solid (174 mg, 73%).[29] IR ν_{max} 3052, 1566, 1523, 1461, 1361, 1156, 860 cm^{-1}. HRESMS found: (M + H) 354.1917; $C_{19}H_{23}N_5O_2$ requires (M + H), 354.1930. ^{1}H NMR (DMSO) δ 11.10 (1H, t), 11.00 (1H, t), 9.45 (1H, s), 8.97 (1H, d), 8.05 (1H, d),

7.70 (6H, bs), 7.58 (2H, s), 6.00 (4H, s), 3.63−3.56 (4H, m), 2.90 (4H, t), 1.97−1.89 (4H, m). LCMS: T_r = solvent front, 95% purity; m/z (%) = 354 (95), $[M + H]^+$ 325 (100).

6,9-Bis(4-aminobutylamino)benzo[g]isoquinoline-5,10-dione Dihydrochloride 9. A mixture of the difluoro dione **16** (75 mg, 0.31 mmol) and 1,4-diaminobutane (297 μL, 3.1 mmol) in THF (5 mL) was stirred at 50 °C for 20 h. The solution was cooled and the precipitate was filtered off and washed with THF. The filtrate was concentrated in vacuo and the residue dried under a stream of nitrogen to aid in removal of excess amine. The residue was dissolved in MeOH (2 mL), and a solution of 1.25 N HCl in MeOH (1.86 mmol) was added. A sufficient volume of EtOAc was added, and a precipitate developed. The solid was filtered off and washed with EtOAc to afford the dihydrochloride **9** as a dark-blue solid (90 mg, 67%).[29] IR ν_{max} 2934, 1568, 1531, 1279, 1174, 838 cm^{-1}. HRESMS found: (M + H) 382.2246; $C_{21}H_{27}N_5O_2$ requires (M + H), 382.2243. ^1H NMR (DMSO) δ 11.20 (1H, t), 11.10 (1H, t), 9.44 (1H, s), 8.95 (1H, d), 8.05 (1H, d), 7.85 (6H, bs), 7.59 (2H, s), 3.60−3.50 (4H, m), 2.90−2.80 (4H, m), 1.75−1.65 (8H, m). LCMS: T_r = 4.29, 95% purity; m/z (%) = 381 (2.5), $[M + H]^+$ 311 (50), 240 (100).

6,9-Bis(5-aminopentylamino)benzo[g]isoquinoline-5,10-dione Dihydrochloride 10. A mixture of the difluoro dione **16** (75 mg, 0.31 mmol) and 1,5-diaminopentane (360 μL, 3.1 mmol) in THF (5 mL) was stirred at 50 °C for 20 h. The solution was cooled, and the precipitate was filtered off and washed with THF. The filtrate was concentrated in vacuo and the residue dried under a stream of nitrogen to aid in removal of excess amine. The residue was dissolved in MeOH (2 mL), and a solution of 1.25 N HCl in MeOH (1.86 mmol) was added. A sufficient volume of EtOAc was added, and a precipitate developed. The solid was filtered off and washed with EtOAc to yield the dihydrochloride **10** as a dark-blue solid (70 mg, 51%). IR ν_{max} 2934, 1573, 1391, 1171, 830 cm^{-1}. HRESMS found: (M − H) 408.2387; $C_{23}H_{31}N_5O_2$ requires (M − H), 408.2400. ^1H NMR (DMSO) δ 11.27 (1H, bs), 11.14 (1H, bs), 9.45 (1H, s), 8.95 (1H, d), 8.09 (1H, d), 7.95 (6H, bs), 7.59 (2H, s), 3.55−3.45 (4H, m), 2.85−2.75 (4H, m), 1.71−1.60 (8H, m), 1.50−1.45 (4H, m). LCMS: T_r = solvent front, 95% purity; m/z (%) = 409 (10), $[M + H]^+$ 325 (100).

Acknowledgment. This work was supported by grants from the National Health and Medical Research Council, Australia (grant number 487333) (S.M.C., D.R.P., and K.G.W.) and CASS Foundation, Melbourne, Australia (grant number SM/08/1971) (S.M.C., B.E.).

Supporting Information Available: The full data set for DNA sequence specificity of all anthracenedione derivatives. This material is available free of charge via the Internet at http://pubs.acs.org.

References

(1) Beljanski, V.; Marzilli, L. G.; Doetsch, P. W. DNA damage-processing pathways involved in the eukaryotic cellular response to anticancer DNA cross-linking drugs. *Mol. Pharmacol.* **2004**, *65*, 1496–1506.
(2) Goldenberg, G.Tannock, I.Drug resistance and experimental chemotherapy. In *The Basic Science of Oncology*; McGraw-Hill: New York 1998; pp 392−419
(3) Feofanov, A.; Sharonov, S.; Kudelina, I.; Fleury, F.; Nabiev, I. Localization and molecular interactions of mitoxantrone within living K562 cells as probed by confocal spectral imaging analysis. *Biophys. J.* **1997**, *73*, 3317–3327.
(4) Feofanov, A.; Sharonov, S.; Fleury, F.; Kudelina, I.; Nabiev, I. Quantitative confocal spectral imaging analysis of mitoxantrone within living K562 cells: intracellular accumulation and distribution of monomers, aggregates, naphtoquinoxaline metabolite, and drug-target complexes. *Biophys. J.* **1997**, *73*, 3328–3336.
(5) De Vita, V. T.; Hellman, S.; Rosenberg, S. A. *Cancer—Principles and Practice of Oncology*; J.B. Lippincott: Philadelphia, PA, 1993.
(6) Cornbleet, M. A.; Stuart-Harris, R. C.; Smith, I. E.; Coleman, R. E.; Rubens, R. D.; McDonald, M.; Mouridsen, H. T.; Rainer, H.; van Oosterom, A. T.; Smyth, J. F. Mitoxantrone for the treatment of advanced breast cancer: single-agent therapy in previously untreated patients. *Eur. J. Cancer Clin. Oncol.* **1984**, *20*, 1141–1146.
(7) Durr, F. E. *Anthracyclines and Anthracenedione-Based Anticancer Agents*; Elsevier: Amsterdam, 1988.
(8) Pratt, W. B.; Ruddon, R. W.; Ensminger, W. D.; Maybaum, J. *The Anticancer Drugs*; Oxford University Press: New York, 1994.
(9) Burden, D. A.; Osheroff, N. Mechanism of action of eukaryotic topoisomerase II and drugs targeted to the enzyme. *Biochim. Biophys. Acta* **1998**, *1400*, 139–154.
(10) Faulds, D.; Balfour, J. A.; Chrisp, P.; Langtry, H. D. Mitoxantrone. A review of its pharmacodynamic and pharmacokinetic properties, and therapeutic potential in the chemotherapy of cancer. *Drugs* **1991**, *41*, 400–449.
(11) Parker, B. S.; Cutts, S. M.; Cullinane, C.; Phillips, D. R. Formaldehyde activation of mitoxantrone yields CpG and CpA specific DNA adducts. *Nucleic Acids Res.* **2000**, *28*, 982–990.
(12) Parker, B. S.; Cullinane, C.; Phillips, D. R. Formation of DNA adducts by formaldehyde-activated mitoxantrone. *Nucleic Acids Res.* **1999**, *27*, 2918–2923.
(13) Zeman, S. M.; Phillips, D. R.; Crothers, D. M. Characterization of covalent adriamycin-DNA adducts. *Proc. Natl Acad. Sci. U.S.A.* **1998**, *95*, 11561–11565.
(14) Thorndike, J.; Beck, W. S. Production of formaldehyde from N5-methyltetrahydrofolate by normal and leukemic leukocytes. *Cancer Res.* **1977**, *37*, 1125–1132.
(15) Taatjes, D. J.; Gaudiano, G.; Resing, K.; Koch, T. H. Redox pathway leading to the alkylation of DNA by the anthracycline, antitumor drugs adriamycin and daunomycin. *J. Med. Chem.* **1997**, *40*, 1276–1286.
(16) Taatjes, D. J.; Gaudiano, G.; Koch, T. H. Production of formaldehyde and DNA−adriamycin or DNA−daunomycin adducts, initiated through redox chemistry of dithiothreitol/iron, xanthine oxidase/NADH/iron, or glutathione/iron. *Chem. Res. Toxicol.* **1997**, *10*, 953–961.
(17) Parker, B. S.; Buley, T.; Evison, B. J.; Cutts, S. M.; Neumann, G. M.; Iskander, M. N.; Phillips, D. R. A molecular understanding of mitoxantrone−DNA adduct formation: effect of cytosine methylation and flanking sequences. *J. Biol. Chem.* **2004**, *279*, 18814–18823.
(18) Cutts, S. M.; Nudelman, A.; Rephaeli, A.; Phillips, D. R. The power and potential of doxorubicin−DNA adducts. *IUBMB Life* **2005**, *57*, 73–81.
(19) Cutts, S. M.; Nudelman, A.; Pillay, V.; Spencer, D. M.; Levovich, I.; Rephaeli, A.; Phillips, D. R. Formaldehyde-releasing prodrugs in combination with adriamycin can overcome cellular drug resistance. *Oncol. Res.* **2005**, *15*, 199–213.
(20) Wang, A. H.; Gao, Y. G.; Liaw, Y. C.; Li, Y. K. Formaldehyde cross-links daunorubicin and DNA efficiently: HPLC and X-ray diffraction studies. *Biochemistry* **1991**, *30*, 3812–3815.
(21) Bailly, C.; Goossens, J. F.; Laine, W.; Anizon, F.; Prudhomme, M.; Ren, J.; Chaires, J. B. Formaldehyde-induced alkylation of a 2′-aminoglucose rebeccamycin derivative to both A.T and G.C base pairs in DNA. *J. Med. Chem.* **2000**, *43*, 4711–4720.
(22) Borchmann, P.; Reiser, M. Pixantrone (Novuspharma). *Idrugs* **2003**, *6*, 486–490.
(23) Beggiolin, G.; Crippa, L.; Menta, E.; Manzotti, C.; Cavalletti, E.; Pezzoni, G.; Torriani, D.; Randisi, E.; Cavagnoli, R.; Sala, F.; Giuliani, F. C.; Spinelli, S. Bbr 2778, an aza-anthracenedione endowed with preclinical anticancer activity and lack of delayed cardiotoxicity. *Tumori* **2001**, *87*, 407–416.
(24) Evison, B. J.; Mansour, O. C.; Menta, E.; Phillips, D. R.; Cutts, S. M. Pixantrone can be activated by formaldehyde to generate a potent DNA adduct forming agent. *Nucleic Acids Res.* **2007**, *35*, 3581–3589.
(25) Evison, B. J.; Chiu, F.; Pezzoni, G.; Phillips, D. R.; Cutts, S. M. Formaldehyde-activated Pixantrone is a monofunctional DNA alkylator that binds selectively to CpG and CpA doublets. *Mol. Pharmacol.* **2008**, *74*, 184–194.
(26) Nudelman, A.; Ruse, M.; Aviram, A.; Rabizadeh, E.; Shaklai, M.; Zimrah, Y.; Rephaeli, A. Novel anticancer prodrugs of butyric acid. 2. *J. Med. Chem.* **1992**, *35*, 687–694.
(27) Cullinane, C.; Phillips, D. R. Thermal stability of DNA adducts induced by cyanomorpholinoadriamycin in vitro. *Nucleic Acids Res.* **1993**, *21*, 1857–1862.
(28) Krapcho, A. P.; Getahun, Z.; Avery, K. J. The Synthesis of 1,4-Difluoro-5,8-Dihydroxyanthracene-9,10-Dione and Ipso Substitutions of the Fluorides by Diamines Leading to 1,4-Bis-[(Aminoalkyl)-Amino]-5,8-Dihydroxyanthracene-9,10-Diones. *Synth. Commun.* **1990**, *20*, 2139–2146.
(29) Krapcho, A. P.; Petry, M. E.; Getahun, Z.; Landi, J. J., Jr.; Stallman, J.; Polsenberg, J. F.; Gallagher, C. E.; Maresch, M. J.; Hacker, M. P.;

Giuliani, F. C.; Beggiolin, G.; Pezzoni, G.; Menta, E; Manzotti, C.; Oliva, A.; Spinelli, S.; Tognella, S. 6,9-Bis[(aminoalkyl)amino]-benzo[g]isoquinoline-5,10-diones. A novel class of chromophore-modified antitumor anthracene-9,10-diones: synthesis and antitumor evaluations. *J. Med. Chem.* **1994**, *37*, 828–837.
(30) De Isabella, P.; Palumbo, M.; Sissi, C.; Capranico, G.; Carenini, N.; Menta, E.; Oliva, A.; Spinelli, S.; Krapcho, A. P.; Giuliani, F. C.; Zunino, F. Topoisomerase II DNA cleavage stimulation, DNA binding activity, cytotoxicity, and physicochemical properties of 2-aza- and 2-aza-oxide-anthracenedione derivatives. *Mol. Pharmacol.* **1995**, *48*, 30–38.
(31) Askirka, V. F.; Maskevich, A. A.; Stepuro, V. I.; Maskevich, S. A. Luminescent properties of mitoxantrone in different microsurroundings. *J. Appl. Spectrosc.* **2004**, *71*, 39–43.
(32) Jones, G. B.; Palumbo, M. *Advances in DNA Sequence-Specific Agents*, Vol. 3; JAI Press Inc: London, 1998.
(33) Hurley, L. H. DNA and its associated processes as targets for cancer therapy. *Nature Rev. Cancer* **2002**, *2*, 188–200.
(34) Phillips, D. R.; Cullinane, C. Adriamycin. *Encyclopedia of Molecular Biology*: John Wiley & Sons: New York, 1999; pp 68−72.
(35) Panousis, C.; Phillips, D. R. DNA sequence specificity of mitoxantrone. *Nucleic Acids Res.* **1994**, *22*, 1342–1345.
(36) Lawley, P. D. Effects of some chemical mutagens and carcinogens on nucleic acids. *Prog. Nucleic Acid Res.* **1966**, *5*, 89–131.
(37) Hemminki, K.; Ludlum, D. B. Covalent modification of DNA by antineoplastic agents. *J. Natl. Cancer Inst.* **1984**, *73*, 1021–1028.
(38) Hartley, J. A.; Lown, J. W.; Mattes, W. B.; Kohn, K. W. DNA sequence specificity of antitumor agents. Oncogenes as possible targets for cancer therapy. *Acta Oncol.* **1988**, *27*, 503–510.
(39) Saxonov, S.; Berg, P.; Brutlag, D. L. A genome-wide analysis of CpG dinucleotides in the human genome distinguishes two distinct classes of promoters. *Proc. Natl. Acad. Sci. U.S.A.* **2006**, *103*, 1412–1417.
(40) Jones, P. A.; Baylin, S. B. The fundamental role of epigenetic events in cancer. *Nature Rev. Genet.* **2002**, *3*, 415–428.
(41) Gardiner-Garden, M.; Frommer, M. CpG islands in vertebrate genomes. *J. Mol. Biol.* **1987**, *196*, 261–282.
(42) Fatemi, M.; Pao, M. M.; Jeong, S.; Gal-Yam, E. N.; Egger, G.; Weisenberger, D. J.; Jones, P. A. Footprinting of mammalian promoters: use of a CpG DNA methyltransferase revealing nucleosome positions at a single molecule level. *Nucleic Acids Res.* **2005**, *33*, e176.
(43) Cutts, S. M.; Rephaeli, A.; Nudelman, A.; Hmelnitsky, I.; Phillips, D. R. Molecular basis for the synergistic interaction of adriamycin with the formaldehyde-releasing prodrug pivaloyloxymethyl butyrate (AN-9). *Cancer Res.* **2001**, *61*, 8194–8202.
(44) Batova, A.; Shao, L. E.; Diccianni, M. B.; Yu, A. L.; Tanaka, T.; Rephaeli, A.; Nudelman, A.; Yu, J. The histone deacetylase inhibitor AN-9 has selective toxicity to acute leukemia and drug-resistant primary leukemia and cancer cell lines. *Blood* **2002**, *100*, 3319–3324.
(45) Vigushin, D. M.; Coombes, R. C. Histone deacetylase inhibitors in cancer treatment. *Anti-Cancer Drug* **2002**, *13*, 1–13.
(46) Cress, W. D.; Seto, E. Histone deacetylases, transcriptional control, and cancer. *J. Cell. Physiol.* **2000**, *184*, 1–16.
(47) Marks, P.; Rifkind, R. A.; Richon, V. M.; Breslow, R.; Miller, T.; Kelly, W. K. Histone deacetylases and cancer: causes and therapies. *Nature Rev. Cancer* **2001**, *1*, 194–202.
(48) Nolan, L.; Johnson, P. W.; Ganesan, A.; Packham, G.; Crabb, S. J. Will histone deacetylase inhibitors require combination with other agents to fulfil their therapeutic potential? *Br. J. Cancer* **2008**, *99*, 689–694.
(49) Kim, M. S.; Blake, M.; Baek, J. H.; Kohlhagen, G.; Pommier, Y.; Carrier, F. Inhibition of histone deacetylase increases cytotoxicity to anticancer drugs targeting DNA. *Cancer Res.* **2003**, *63*, 7291–7300.
(50) Phillips, D. R.; Cullinane, C. M.; Crothers, D. M. An in vitro transcription assay for probing drug−DNA interactions at individual drug sites. *Mol. Biotechnol.* **1998**, *10*, 63–75.
(51) Phillips, D. R.; Cutts, S. M.; Cullinane, C. M.; Crothers, D. M. High-resolution transcription assay for probing drug−DNA interactions at individual drug sites. *Method. Enzymol.* **2001**, *340*, 466–485.
(52) Chou, T. C.; Talalay, P. Quantitative analysis of dose−effect relationships: the combined effects of multiple drugs or enzyme inhibitors. *Adv. Enzyme Regul.* **1984**, *22*, 27–55.
(53) Murdock, K. C.; Child, R. G.; Fabio, P. F.; Angier, R. B.; Wallace, R. E.; Durr, F. E.; Citarella, R. V. Antitumor agents. 1. 1,4-Bis-[(aminoalkyl)amino]-9,10-anthracenediones. *J. Med. Chem.* **1979**, *22*, 1024–1030.